

Topological Residual Asymmetry for Bivariate Causal Direction

Mouad El Bouchattaoui^{* 1}

Abstract

Inferring causal direction from purely observational bivariate data is fragile: many methods commit to a direction even in ambiguous or near non-identifiable regimes. We propose *Topological Residual Asymmetry* (TRA), a geometry-based criterion for additive-noise models. TRA compares the shapes of two cross-fitted regressor–residual clouds after rank-based copula standardization: in the correct direction, residuals are approximately independent, producing a two-dimensional bulk, while in the reverse direction—especially under low noise—the cloud concentrates near a one-dimensional tube. We quantify this bulk–tube contrast using a 0D persistent-homology functional, computed efficiently from Euclidean MST edge-length profiles. We prove consistency in a triangular-array small-noise regime, extend the method to fixed noise via a binned variant (TRA-s), and introduce TRA-C, a confounding-aware abstention rule calibrated by a Gaussian-copula plug-in bootstrap. Extensive experiments across many challenging synthetic and real-data scenarios demonstrate the method’s superiority.

1. Introduction

Inferring causal direction from observational data remains a central challenge in statistics and machine learning: for two real-valued variables (X, Y) , dependence alone cannot distinguish $X \rightarrow Y$, $Y \rightarrow X$, or *no orientation* without structural assumptions (Spirtes et al., 2001; Pearl, 2009). Identifiability is obtained by restricting the data-generating class, e.g. via additive-noise models (ANMs), where the causal direction admits $Y = f(X) + \varepsilon$ with $\varepsilon \perp\!\!\!\perp X$ while the reverse representation typically fails (Hoyer et al., 2009; Peters et al., 2014), or via other asymmetry principles such as information-geometric criteria linking the cause marginal to local expansion of the mechanism (Janzing et al., 2012). Most practical bivariate methods instant-

¹Paris, France. Correspondence to: Mouad El Bouchattaoui <mouad.elbouchattaoui@gmail.com>.

tiate these asymmetries by fitting both directions and comparing scalar scores, e.g., regress-then-test ANM pipelines (RESIT), information-geometric scores (IGCI), regression-error asymmetries (RECI), and minimum description length (MDL)/regularized-regression proxies (SLOPPY) (Mooij et al., 2016; Glymour et al., 2019). However, such summaries can be brittle under finite samples or mild misspecification and often provide limited insight into *why* a direction is preferred (Mooij et al., 2016; Zhang et al., 2012); moreover, in near non-identifiable regimes (e.g., close to linear-Gaussian) they may still force a decision despite weak evidence rather than signaling ambiguity (Hoyer et al., 2009; Peters et al., 2014).

We take a complementary view: in ANMs, direction is encoded in the *geometry* of the fitted regressor–residual cloud. In the causal direction, residuals are (asymptotically) independent of the regressor under consistent regression, as the ANM constraint requires (Hoyer et al., 2009; Peters et al., 2014). In the reverse direction, an independent-noise representation occurs only in special non-identifiable cases (e.g., linear-Gaussian) (Hoyer et al., 2009; Peters et al., 2014), so residuals remain generically dependent and, in low-noise injective settings, often nearly functional: the reverse cloud concentrates near a low-dimensional set (typically a smooth curve) while the causal cloud retains a two-dimensional bulk. A copula transform (Nelsen, 2006) makes this contrast invariant to monotone marginal reparameterizations.

We introduce *Topological Residual Asymmetry* (TRA), a directional score that compares the shapes of the two fitted residual clouds. TRA first applies a rank-based copula standardization, making the comparison invariant to strictly increasing marginal transformations and therefore sensitive only to copula-level dependence. It then summarizes each cloud with a 0D persistent-homology functional (Edelsbrunner et al., 2002; Ghrist, 2008). For the standard union-of-balls (distance-to-set) filtration, the 0D merge scales coincide with the single-linkage hierarchy and can be read directly from Euclidean *minimum-spanning-tree* (MST) edge lengths (up to 1/2 radius factor) (Gower & Ross, 1969). These MST-based summaries serve as a practical proxy for intrinsic dimension via scaling laws for geometric graph functionals (Steele, 1988; Penrose, 2003; Costa & Hero, 2004a), with proven stability under perturbations (Cohen-Steiner et al., 2007).

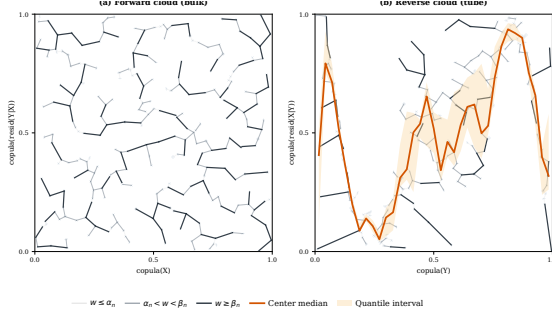


Figure 1. Bulk-tube contrast in copula transform. Forward clouds are 2D, while reverse clouds collapse near a curve. $Y_{n,i} | X_i \sim \mathcal{N}(X_i^3, n^{-1/2})$, $n = 250$

Finally, we introduce *TRA-C*, a confounding-aware version of TRA with abstention. Under a symmetric *no-direction* null—dependence without causal asymmetry—the signed score concentrates near zero, so TRA-C abstains; when the observed asymmetry is atypical under the fitted null, TRA-C returns its sign. Implementations of all models, baselines, and experiments are provided in the supplementary material.

2. Related Work

Many bivariate orientation methods exploit an *asymmetry principle*: a property that holds (approximately) in the true direction and fails except in special non-identifiable cases. They orient by comparing direction-specific scores, often favoring the direction that admits a *simpler* or more *generic* explanation. IGCI targets near-deterministic mechanisms and, under an independence-of-cause-and-mechanism view, links the cause density to local expansion of the transfer function (Janzing et al., 2012). RECI compares directions via regression error (Blöbaum et al., 2018), while MDL-inspired methods such as SLOPPY use description-length surrogates from local/global regression fits (Marx & Vreeken, 2019). Kernel and distributional criteria such as KCDC and CDCI contrast direction-specific conditional-distribution complexity (Mitrović et al., 2018; Duong & Nguyen, 2022), and quantile diagnostics such as bQCD compare multiple conditional quantiles to capture changing conditional shape, including heteroscedasticity (Tagasovska et al., 2020). TRA fits within this family but differs in the object it compares: rather than a single slope, error, or divergence statistic, it contrasts the *multiscale geometry of residual point clouds*. Moreover, TRA operates on *copula-standardized* residual clouds, so the relevant geometry reflects the *dependence structure* (copula geometry) rather than marginal scale.

A key identifiable model class is the ANM. Under suitable regularity conditions, this identifies the causal direction except in known non-identifiable settings (notably some linear-Gaussian families) (Hoyer et al., 2009; Peters et al., 2014). In practice, ANM methods regress in both directions and select the one in which the residuals are most consistent

with independence from the regressor, using dependence measures such as HSIC or conditional-independence tests such as KCI (Gretton et al., 2005; Zhang et al., 2012). RE-SIT extends this regress-then-test idea to multivariate DAG learning; in the bivariate case, it reduces to an ANM-style orientation rule (Peters et al., 2014). TRA departs from this template in what it extracts from residuals: rather than scoring residual (in)dependence directly, it summarizes the *geometry of the residual point cloud*.

TRA’s functional is closely related to intrinsic-dimension and manifold-diagnostics methods, where nearest-neighbor graphs and MSTs yield statistics for detecting low-dimensional structure or estimating dimension via scaling laws (Costa & Hero, 2004b; Camastra, 2016). After copula standardization, TRA exploits this multiscale spacing to contrast “bulk-like” and “curve-like” residual clouds. Rather than estimating a global intrinsic dimension for exploration, TRA uses an MST-persistence functional as a *directional asymmetry diagnostic* for causal orientation, with an explicit abstention option when separation is unreliable.

A separate line of work treats bivariate orientation as supervised learning on labeled cause–effect pairs. RCC trains a classifier on randomized feature maps of empirical distributions (Lopez-Paz et al., 2015), while NCC learns end-to-end representations, typically from synthetic and/or curated pairs (Lopez-Paz et al., 2017); support-measure machines similarly embed each dataset as a probability measure and apply kernels on measures (Varando et al., 2024). In parallel, generative and compression-based methods compare direction-specific explanations, including CGNN-style generative modeling (Goudet et al., 2018), nonlinear-ICA ensembles such as Causal Mosaic (Wu & Fukumizu, 2020), and variational Bayesian compression (Tran et al., 2025).

3. Theoretical Setup

For this section, we defer detailed proofs of all theoretical claims to Appendix B. All notions from metric geometry and geometric graphs used in the proofs are recalled in the Background (Appendix A). We work in the bivariate setting and, for each n , observe n *row-wise i.i.d.* samples $\mathcal{D}_n := \{(X_i, Y_{n,i})\}_{i=1}^n$. To cover both fixed- and vanishing-noise regimes, we consider the additive-noise model (Hoyer et al., 2009; Peters et al., 2014):

$$Y_{n,i} = f(X_i) + \sigma_n \varepsilon_i, \quad \varepsilon_i \perp\!\!\!\perp X_i, \quad \mathbb{E}[\varepsilon_i] = 0, \quad \sigma_n \geq 0 \quad (1)$$

Here $(X_i, \varepsilon_i)_{i=1}^n$ are i.i.d., while σ_n may depend on n . The *fixed-noise* regime has $\sigma_n \equiv \sigma > 0$, whereas the *small-noise* regime assumes $\sigma_n \downarrow 0$ as $n \rightarrow \infty$. In the forward (putatively causal) direction, the regression function is f . In the reverse direction, set $m_n(y) := \mathbb{E}[X | Y_n = y]$, which may vary with n through σ_n .

Fix an integer $K \geq 2$ and a deterministic K -fold parti-

tion $\{I_k\}_{k=1}^K$ of $[n]$ (Chernozhukov et al., 2018); write $k(i)$ for the unique index such that $i \in I_{k(i)}$. For each fold k , fit forward and backward regressors $\hat{f}_n^{(-k)}$ and $\hat{g}_n^{(-k)}$ on the training set $\{(X_j, Y_{n,j})\}_{j \notin I_k}$. Define the out-of-fold residuals $r_i^{(Y|X)} := Y_{n,i} - \hat{f}_n^{(-k(i))}(X_i)$ and $r_i^{(X|Y)} := X_i - \hat{g}_n^{(-k(i))}(Y_{n,i})$. Their oracle counterparts replace the estimators by the population targets f and m_n : $r_{i,o}^{(Y|X)} := Y_{n,i} - f(X_i)$ and $r_{i,o}^{(X|Y)} := X_i - m_n(Y_{n,i})$. For any direction $A|B$, write $\mathcal{R}_{A|B} := \{(B_i, r_i^{(A|B)})\}_{i=1}^n$, and define $\mathcal{R}_{o,A|B}^{(n)}$ analogously using oracle residuals. In particular, $\mathcal{R}_{Y|X}^{(n)} = \{(X_i, r_i^{(Y|X)})\}_{i=1}^n$ and $\mathcal{R}_{X|Y}^{(n)} = \{(Y_{n,i}, r_i^{(X|Y)})\}_{i=1}^n$, similarly for $\mathcal{R}_{o,Y|X}^{(n)}$ and $\mathcal{R}_{o,X|Y}^{(n)}$.

Copula standardization. Our goal is to compare the *dependence geometry* of the forward and reverse residual clouds. Doing so directly in \mathbb{R}^2 is often fragile: marginal features—scale, skewness, heavy tails, or heteroscedasticity—can dominate Euclidean geometry even when the underlying dependence is unchanged. Copula coordinates mitigate this nuisance by applying the marginal CDF to each coordinate (Nelsen, 2006).

For a pair (U, V) with continuous marginals, define $T_{U,V}(u, v) := (F_U(u), F_V(v)) \in [0, 1]^2$. In the oracle construction we copula-standardize each direction separately: $\tilde{\mathcal{R}}_{Y|X}^{(n)} := T_{X, r_{o,Y|X}^{(n)}}(\mathcal{R}_{o,Y|X}^{(n)})$ and $\tilde{\mathcal{R}}_{X|Y}^{(n)} := T_{Y_{n,r_{o,X|Y}^{(n)}}}(\mathcal{R}_{o,X|Y}^{(n)})$. In practice, the marginal CDFs are unknown, so we replace them by ranks (Fermanian et al., 2004). For a univariate sample $(U_i)_{i=1}^n$, define $T_n(U_i) := \text{rank}(U_i)/(n+1)$. Applying T_n coordinatewise gives the empirical copula-standardized clouds

$$\tilde{\mathcal{R}}_{Y|X}^{(n)} := T_n(\mathcal{R}_{Y|X}^{(n)}), \quad \tilde{\mathcal{R}}_{X|Y}^{(n)} := T_n(\mathcal{R}_{X|Y}^{(n)}).$$

We view a cloud $\mathcal{R} = \{\mathbf{Z}_1, \dots, \mathbf{Z}_n\} \subset \mathbb{R}^2$ as a finite metric space with distance $\|\cdot\|_2$. The *Euclidean minimum spanning tree* (MST) $\text{MST}(\mathcal{R})$ is the graph on vertex set \mathcal{R} that connects all points with $n-1$ edges and minimizes the total edge weight, where the weight of an edge $e = (\mathbf{Z}_i, \mathbf{Z}_j)$ is its Euclidean length $w(e) := \|\mathbf{Z}_i - \mathbf{Z}_j\|_2$ (Kruskal, 1956; Gower & Ross, 1969). We write the multiset of MST edge weights as

$$\{\ell_j(\mathcal{R})\}_{j=1}^{n-1} := \{w(e) : e \in \text{MST}(\mathcal{R})\}.$$

Mesoscopic scale: separating “bulk” from “curve”. After copula standardization, each residual cloud forms a point set \mathcal{R} . We define the local separation scale as the typical interpoint distance, which we can represent by the nearest-neighbor (NN) distances

$$d_i := \min_{j \neq i} \|\mathbf{Z}_i - \mathbf{Z}_j\|_2.$$

A comparable notion of local scale is provided by *typical* Euclidean MST edge lengths on \mathcal{R} (the MST contains many edges at nearest-neighbor scale, though it may also include longer bridging edges).

This local separation reflects the *intrinsic dimension* of the support. For a genuinely d -dimensional cloud with a density bounded away from 0 and ∞ on a set of positive d -volume, typical NN distances scale as $\Theta(n^{-1/d})$ (e.g. in probability), hence as $\Theta(n^{-1/2})$ in $d=2$ (Penrose & Yukich, 2009). Moreover, for i.i.d. samples in \mathbb{R}^d , the total Euclidean MST length scales as $\Theta(n^{(d-1)/d})$, so the *average* MST edge length is $\Theta(n^{-1/d})$ (Seo & Yukich, 2000). In contrast, if the cloud is supported on a one-dimensional C^1 curve and sampled i.i.d. with a density bounded away from 0 along arclength, local separations scale as $\Theta(n^{-1})$, and the maximal spacing along the curve is $\Theta((\log n)/n)$ almost surely (Devroye, 1981). These two scales motivate a mesoscopic window α_n lying strictly between $n^{-1/2}$ and n^{-1} , separating “bulk-like” from “curve-like” geometry:

$$\frac{\log n}{n} = o(\alpha_n), \quad n^{-1} \ll \alpha_n \ll n^{-1/2}, \quad \beta_n \asymp \alpha_n. \quad (2)$$

We use the concrete choice

$$\alpha_n = \kappa n^{-2/3}, \quad \beta_n = c_\beta \alpha_n, \quad \kappa > 0, \quad c_\beta > 1, \quad (3)$$

which satisfies (2). At this scale, bulk clouds still look “thick” with many MST edges exceeding α_n , whereas curve-like clouds already look “tight” with most edges falling below α_n . To measure how much connectivity happens *inside* $[\alpha, \beta]$, define the soft window

$$\Psi_{\alpha,\beta}(t) := (\min\{t, \beta\} - \alpha)_+ \in [0, \beta - \alpha], \quad (4)$$

and, for a cloud \mathcal{R} of size $n \geq 2$, the score

$$\overline{\text{TP}}_0^{[\alpha, \beta]}(\mathcal{R}) := \frac{1}{(n-1)(\beta - \alpha)} \sum_{e \in \text{MST}(\mathcal{R})} \Psi_{\alpha,\beta}(w(e)). \quad (5)$$

where $w(e) = \|\mathbf{Z}_i - \mathbf{Z}_j\|_2$ denotes the Euclidean length of the edge $e = (\mathbf{Z}_i, \mathbf{Z}_j)$. Large values of $\overline{\text{TP}}_0^{[\alpha, \beta]}$ mean many MST edges lie above α (bulk-like at that scale); values near 0 mean most merges occur below α (tube-like at that scale).

Definition 3.1 (TRA score and direction). Define the normalized TRA score

$$\Delta_n := \overline{\text{TP}}_0^{[\alpha_n, \beta_n]}(\tilde{\mathcal{R}}_{Y|X}^{(n)}) - \overline{\text{TP}}_0^{[\alpha_n, \beta_n]}(\tilde{\mathcal{R}}_{X|Y}^{(n)}) \in [-1, 1]. \quad (6)$$

We predict $X \rightarrow Y$ if $\Delta_n > 0$ and $Y \rightarrow X$ if $\Delta_n < 0$.

Core intuition. In an ANM, the forward residual is (approximately) independent of the cause (Peters et al., 2014), and the standardized forward cloud behaves like a genuinely two-dimensional scatter in $[0, 1]^2$. In the reverse direction, in low-noise injective settings the reverse residual becomes

nearly deterministic in Y , so the standardized reverse cloud concentrates around a curve (a thin tube). TRA detects this contrast at the intermediate window $[\alpha_n, \beta_n]$: bulk clouds yield larger $\overline{\text{TP}}_0^{[\alpha_n, \beta_n]}$ than tube-like clouds, hence the sign of Δ_n reveals the direction.

The bulk–tube heuristic becomes a theorem once we control two effects: (i) the small-noise geometry of the *oracle* copula clouds; and (ii) perturbations from cross-fitted regression and rank–copula standardization at the mesoscopic scale α_n . We package the required conditions in three assumptions.

Assumption 3.2 (Forward Model regularity). X is supported on a compact interval $I = [a, b]$, and $f : I \rightarrow \mathbb{R}$ is C^1 . There exist $J \geq 1$ and breakpoints $a = t_0 < t_1 < \dots < t_J = b$ such that on each $I_j := (t_{j-1}, t_j)$, f is strictly monotone and

$$0 < c_f \leq |f'(x)| \leq C_f \quad (x \in I_j, j = 1, \dots, J).$$

Let $\mathcal{V} := \{f(t_1), \dots, f(t_{J-1})\}$ be the turning-value set. The noise ε has a continuous density and is sub-Gaussian, hence $\max_{1 \leq i \leq n} |\varepsilon_i| = O_{\mathbb{P}}(\sqrt{\log n})$.

Assumption 3.3 (Reverse target regularity). Fix $\eta \in [0, 1]$. There exists a compact interval $J_\eta \Subset f(I) \setminus \mathcal{V}$ such that $\mathbb{P}(Y_n \in J_\eta) \rightarrow 1$, the density p_{Y_n} is uniformly bounded below on J_η , and m_n is uniformly continuous on J_η uniformly in n .

Assumption 3.4 (Estimation error). (i) *Forward L^2 -risk consistency*: $\mathbb{E}\|\widehat{f}_n^{(-k)} - f\|_{L^2(\mathbb{P}_X)}^2 \rightarrow 0$ for each k . (ii) *Reverse uniform-on-test-points consistency on J_η* : for each k , $\delta_n^{(k)} := \max_{i \in I_k: Y_{n,i} \in J_\eta} |\widehat{g}_n^{(-k)}(Y_{n,i}) - m_n(Y_{n,i})| = o_{\mathbb{P}}(\alpha_n)$. (iii) *Noise thickness is negligible*: $\sigma_n \sqrt{\log n} = o(\alpha_n)$.

Remarks. Assumption 3.2 permits global non-invertibility but requires branchwise invertibility with Lipschitz inverse constant $1/c_f$, which controls the thickness of the reverse-direction “tube.” Assumption 3.3 excludes neighborhoods of \mathcal{V} , ensuring the inverse branches are well behaved on J_η . Assumption 3.4 places the scale window $[\alpha_n, \beta_n]$ between the connectivity regimes of the curve and the bulk, and requires both regression error and noise-induced thickness to be $o_{\mathbb{P}}(\alpha_n)$. Together, Assumptions 3.2–3.4 mirror smoothness, tail, and sample-splitting conditions common in ANM identifiability and cross-fitted nuisance estimation; see, e.g., Hoyer et al. (2009); Peters et al. (2014); Chernozhukov et al. (2018); Vershynin (2018).

Theorem 3.5 (Small-noise TRA consistency (normalized score)). *Assume the small-noise ANM $Y_n = f(X) + \sigma_n \varepsilon$ with $\sigma_n \downarrow 0$ and Assumptions 3.2–3.4. Then*

$$\overline{\text{TP}}_0^{[\alpha_n, \beta_n]}(\widetilde{\mathcal{R}}_{Y|X}^{(n)}) \xrightarrow{\mathbb{P}} 1, \quad \overline{\text{TP}}_0^{[\alpha_n, \beta_n]}(\widetilde{\mathcal{R}}_{X|Y}^{(n)}) \xrightarrow{\mathbb{P}} 0.$$

Hence $\Delta_n \xrightarrow{\mathbb{P}} 1$. In particular, for any deterministic threshold $\tau_n \downarrow 0$, the abstaining rule $\widehat{\text{dir}}_n = X \rightarrow Y$ if $\Delta_n > \tau_n$,

$Y \rightarrow X$ if $\Delta_n < -\tau_n$, and abstain otherwise, satisfies

$$\mathbb{P}(\widehat{\text{dir}}_n = X \rightarrow Y) \rightarrow 1, \quad \mathbb{P}(\widehat{\text{dir}}_n = \text{abstain}) \rightarrow 0.$$

3.1. Fixed Noise Regime

In the small-noise regime $\sigma_n \downarrow 0$, the reverse copula cloud becomes one-dimensional at the mesoscopic scale: under branchwise invertibility of f , the reverse oracle cloud concentrates within an $o(\alpha_n)$ -tube around a compact 1-dimensional set $\Gamma_{n,\eta}^\cup$, a finite union of C^1 curves (one per monotone branch). Consequently, all reverse MST merges fall below α_n . However, with fixed noise,

$$Y = f(X) + \varepsilon, \quad \varepsilon \perp\!\!\!\perp X, \quad \text{Var}(\varepsilon) = \sigma^2 > 0,$$

this collapse disappears. Even with the oracle reverse target $m(y) := \mathbb{E}[X \mid Y = y]$, the reverse fluctuation $\xi := X - m(Y)$ satisfies $\mathbb{E}[\xi \mid Y] = 0$ but typically $\text{Var}(\xi \mid Y) = \Theta(1)$. After copula standardization the reverse cloud has $O(1)$ thickness, remains bulk-like, and $\overline{\text{TP}}_0^{[\alpha_n, \beta_n]}$ need not drift to 0.

A smoothed variant, *TRA-s*, recovers a one-dimensional signature by bin-averaging the reverse residuals along the Y -copula coordinate (Tukey, 1961; Cattaneo et al., 2024). Let $U_i := T_n(Y_{n,i}) \in [0, 1]$, and partition $[0, 1]$ into B_n equal bins $I_{n,b} := ((b-1)/B_n, b/B_n]$. Write $J_b := \{i : U_i \in I_{n,b}\}$ and $N_b := |J_b|$. For each nonempty bin, define

$$\bar{u}_b := \frac{1}{N_b} \sum_{i \in J_b} U_i, \quad \bar{r}_b := \frac{1}{N_b} \sum_{i \in J_b} (X_i - \widehat{g}_n^{(-k(i))}(Y_{n,i})),$$

and the binned reverse cloud $\widehat{\mathcal{R}}_{X|Y}^{(n)} := \{(\bar{u}_b, \bar{r}_b) : N_b \geq 1\}$. If $\widehat{g}_n = m$, then \bar{r}_b averages mean-zero fluctuations and typically satisfies $|\bar{r}_b| = O_{\mathbb{P}}(N_b^{-1/2})$, so $\widehat{\mathcal{R}}_{X|Y}^{(n)}$ concentrates near $\Gamma := \{(u, 0) : u \in [0, 1]\}$, up to discretization error $O(B_n^{-1})$ and regression error. Choosing B_n so these terms are $o(\alpha_n)$ makes the binned cloud tube-like at the mesoscopic scale.

Assumptions for TRA-s under fixed noise. TRA-s uses a partitioning smoother (regressogram/binscatter) on the Y -copula axis (Tukey, 1961; Cattaneo et al., 2024). We impose a standard shrinking-bin regime to control bin means uniformly (Györfi et al., 2002), a conditional sub-Gaussian assumption for reverse fluctuations (Vershynin, 2018), and cross-fitting to decouple nuisance estimation from evaluation (Chernozhukov et al., 2018).

Assumption 3.6 (Binning growth rates). With U_i , $I_{n,b}$, J_b , N_b , and $m_n := |\{b : N_b \geq 1\}|$ as above, assume

$$B_n \rightarrow \infty, \quad B_n = o(n), \quad B_n^{7/3} \frac{\log B_n}{n} \rightarrow 0.$$

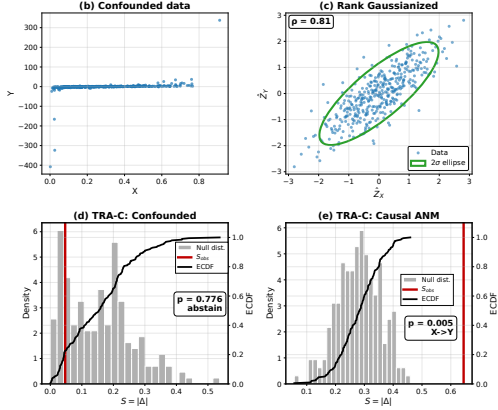


Figure 2. TRA-C calibration on a Gaussian-copula confounding null. Rank-Gaussianized data fit a correlation $\hat{\rho}$ and induce a Gaussian-copula bootstrap for the score Δ_n .

Assumption 3.7 (Conditional reverse fluctuations). Let $m(y) := \mathbb{E}[X \mid Y = y]$ and $\xi := X - m(Y)$. Assume $\|\xi \mid Y = y\|_{\psi_2} \leq K_0\sigma$ for all y in the support of Y .

Assumption 3.8 (Bin-averaged reverse regression error). Let $\hat{g}_n^{(-k)}$ be cross-fitted and let \bar{r}_b be defined as above for bins with $N_b \geq 1$. Set $\tilde{\alpha}_n := \kappa m_n^{-2/3}$ and $\tilde{\beta}_n := c_\beta \tilde{\alpha}_n$. Assume

$$\max_{b: N_b \geq 1} \left| \frac{1}{N_b} \sum_{i \in J_b} (\hat{g}_n^{(-k(i))}(Y_{n,i}) - m(Y_{n,i})) \right| = o_{\mathbb{P}}(\tilde{\alpha}_n).$$

Theorem 3.9 (Fixed-noise TRA-s consistency). Under fixed noise, assume Assumptions 3.2–3.4 and 3.6–3.8. Let $\alpha_n = \kappa n^{-2/3}$, $\beta_n = c_\beta \alpha_n$, let m_n be the number of nonempty bins, and set $\tilde{\alpha}_n = \kappa m_n^{-2/3}$, $\tilde{\beta}_n = c_\beta \tilde{\alpha}_n$. With $\hat{\mathcal{R}}_{X|Y}^{(n)}$ the binned reverse cloud, define

$$\tilde{\Delta}_{0,n} := \overline{\text{TP}}_0^{[\alpha_n, \beta_n]}(\hat{\mathcal{R}}_{Y|X}^{(n)}) - \overline{\text{TP}}_0^{[\tilde{\alpha}_n, \tilde{\beta}_n]}(\hat{\mathcal{R}}_{X|Y}^{(n)}) \in [-1, 1].$$

Then $\overline{\text{TP}}_0^{[\alpha_n, \beta_n]}(\hat{\mathcal{R}}_{Y|X}^{(n)}) \xrightarrow{\mathbb{P}} 1$ and $\overline{\text{TP}}_0^{[\tilde{\alpha}_n, \tilde{\beta}_n]}(\hat{\mathcal{R}}_{X|Y}^{(n)}) \xrightarrow{\mathbb{P}} 0$.

Hence $\Delta_{0,n} \xrightarrow{\mathbb{P}} 1$ and $\mathbb{E}[\tilde{\Delta}_{0,n}] \rightarrow 1$.

3.2. TRA-C: abstention under unobserved confounding via a Gaussian-copula plug-in bootstrap

Theorems 3.9 and 3.5 analyze the base direction scores Δ_n (TRA) and $\tilde{\Delta}_{0,n}$ (TRA-s) under *unconfounded* ANMs. In observational studies, however, the observed dependence may be induced by an *unobserved confounder*, in which case any forced orientation is not causally meaningful (Pearl, 2009; Spirtes et al., 2001). We therefore introduce TRA-C, which equips TRA with an *abstain* option by calibrating the score magnitude against a fitted *confounding-only* null, in the spirit of decision rules with reject options (Chow, 1970; El-Yaniv & Wiener, 2010). Specifically, we test for confounding using the two-sided magnitude $S_n := |\Delta_n|$

for TRA and $S_n := |\tilde{\Delta}_{0,n}|$ for TRA-s. The calibration is otherwise identical; only the definition of S_n differs.

As a toy confounding model, let $H \sim \mathcal{N}(0, 1)$, $Z_X = aH + \xi_X$, $Z_Y = bH + \xi_Y$, with $(\xi_X, \xi_Y) \perp\!\!\!\perp H$ and $(\xi_X, \xi_Y) \sim \mathcal{N}(0, \text{diag}(\sigma_X^2, \sigma_Y^2))$, followed by unknown strictly increasing marginals $X = F_X^{-1}(\Phi(Z_X))$, $Y = F_Y^{-1}(\Phi(Z_Y))$. Figure 2 illustrates the logic of TRA-C: after rank Gaussianization, $(\hat{Z}_X, \hat{Z}_Y) := (\Phi^{-1}(\text{rank}(X)/(n+1)), \Phi^{-1}(\text{rank}(Y)/(n+1)))$ is well approximated by a bivariate normal with $\hat{\rho} \approx 0.81$, yielding an elliptical Gaussian-copula null (shown by the 2σ contour). TRA-C then calibrates the score magnitude $S_n := |\text{Score}_n|$ against this null: under confounding (panel (d)) S_{obs} is typical ($p \approx 0.776$) and TRA-C abstains, while under a genuine ANM (panel (e)) S_{obs} is in the tail ($p \approx 0.005$) and TRA-C returns a direction.

Gaussian-copula null and Gaussianization. As a working “no-direction” dependence baseline, we take \mathcal{M}_0 to be the bivariate Gaussian-copula family: distributions with arbitrary continuous marginals (F_X, F_Y) whose copula is Gaussian, i.e., after marginal Gaussianization $Z_X := \Phi^{-1}(F_X(X))$ and $Z_Y := \Phi^{-1}(F_Y(Y))$, the pair (Z_X, Z_Y) is bivariate normal with correlation $\rho \in (-1, 1)$ (Nelsen, 2006). This removes marginal scales and isolates dependence; under $P \in \mathcal{M}_0$ the *copula* is parameterized by ρ alone, so a plug-in $\hat{\rho}_n$ yields a symmetric baseline for S_n (Liu et al., 2009; Hoff, 2007).

TRA-C calibration. We calibrate $S_n := |\Delta_n|$ (or $S_n := |\tilde{\Delta}_{0,n}|$) under a fitted Gaussian-copula null $\hat{M}_{0,n} = M_{\hat{\rho}_n}$, where $\hat{\rho}_n$ is the correlation of the rank-Gaussianized marginals. Algorithm 1 details the procedure: TRA-C reports a direction only when S_n is extreme under $\hat{M}_{0,n}$, and otherwise abstains. This plug-in parametric-bootstrap calibration in a semiparametric copula model is supported by classical goodness-of-fit validity results (Genest & Rémillard, 2008).

Theorem 3.10 (TRA-C: asymptotic level under a plug-in Gaussian-copula bootstrap). Fix $\alpha \in (0, 1)$. Let $\hat{\rho}_n = \hat{\rho}_n(\mathcal{D}_n)$ be measurable and define the fitted copula null $\hat{M}_{0,n} := M_{\hat{\rho}_n}$. Let $\text{Score}_n \in \{\Delta_n, \tilde{\Delta}_{0,n}\}$ and set $S_n := |\text{Score}_n|$. Conditionally on \mathcal{D}_n , draw a bootstrap sample from $M_{\hat{\rho}_n}$ and compute its analogue S_n^* . Define the conditional bootstrap CDF $\hat{F}_n^*(t) := \Pr_{\hat{\rho}_n}(S_n^* \leq t \mid \mathcal{D}_n)$, $t \in \mathbb{R}$. Let $B_n \rightarrow \infty$ and let $S_n^{*(1)}, \dots, S_n^{*(B)}$ be i.i.d. conditionally on \mathcal{D}_n with conditional CDF \hat{F}_n^* . Define the (conservative) Monte-Carlo p -value

$$\hat{p}_{n, B_n} := \frac{1 + \sum_{b=1}^{B_n} \mathbf{1}\{S_n^{*(b)} \geq S_n\}}{B_n + 1},$$

and the TRA-C rejection (non-abstention) event $R_n :=$

Algorithm 1 TRA-C: Gaussian-copula calibration with abstention

1: **Input:** $\mathcal{D}_n = \{(X_i, Y_i)\}_{i=1}^n$, signed score $\Delta = \text{Score}(\cdot)$, B , α .
 2: Compute $\Delta_n \leftarrow \text{Score}(\mathcal{D}_n)$, $S_n \leftarrow |\Delta_n|$.
 3: Rank-Gaussianize and fit copula correlation: $\hat{Z}_{X,i} \leftarrow \Phi^{-1}(\text{rank}(X_i)/(n+1))$, $\hat{Z}_{Y,i} \leftarrow \Phi^{-1}(\text{rank}(Y_i)/(n+1))$, $\hat{\rho}_n \leftarrow \text{Corr}(\hat{Z}_X, \hat{Z}_Y)$.
 4: **for** $b = 1, \dots, B$ **do**
 5: Draw $(Z_X^*, Z_Y^*) \stackrel{\text{i.i.d.}}{\sim} \mathcal{N}(0, \Sigma(\hat{\rho}_n))$; set $(U_X^*, U_Y^*) = \Phi(Z_X^*, Z_Y^*)$.
 6: $(X^*, Y^*) \leftarrow (\hat{F}_X^{-1}(U_X^*), \hat{F}_Y^{-1}(U_Y^*))$; $S_n^{*(b)} \leftarrow |\text{Score}(\mathcal{D}_n^{*(b)})|$.
 7: **end for**
 8: $\hat{p}_{n,B} \leftarrow \frac{1 + \sum_{b=1}^B \mathbf{1}\{S_n^{*(b)} \geq S_n\}}{B+1}$.
 9: **return** abstain if $\hat{p}_{n,B} > \alpha$, else $\text{sign}(\Delta_n) \in \{X \rightarrow Y, Y \rightarrow X, \text{abstain}\}$.

$\{\hat{p}_{n,B_n} \leq \alpha\}$. Assume that under $P_{\rho_0} \in \mathcal{M}_0$: 1. $\hat{\rho}_n \rightarrow \rho_0$ in P_{ρ_0} -probability; 2. with $F_{\rho_0,n}(t) := \Pr_{\rho_0}(S_n \leq t)$,

$$\sup_{t \in \mathbb{R}} |\hat{F}_n^*(t) - F_{\rho_0,n}(t)| \xrightarrow{P_{\rho_0}} 0;$$

3. $B_n \rightarrow \infty$. Then the TRA-C test has asymptotic level at most α :

$$\limsup_{n \rightarrow \infty} \Pr_{\rho_0}(R_n) \leq \alpha.$$

The guarantee is *relative to the working null* \mathcal{M}_0 . If the data lie in the Gaussian-copula null, then TRA-C outputs a direction with asymptotic probability at most α . We do not claim that all confounded distributions lie in \mathcal{M}_0 ; rather, \mathcal{M}_0 is a broad “dependence-without-direction” family (e.g., latent Gaussian factor structure with unknown monotone marginals), and the plug-in bootstrap prevents directional claims when this null fits.

4. Experiments

Baselines and decision rule. We compare unsupervised, per-pair methods (TRA/TRA-s, RESIT, IGCI, RECI, CDCI, and the per-pair neural compression baseline COMIC) and supervised predictors (RCC, NCC) trained on independent synthetic labeled pairs and evaluated on all Tübingen pairs. For any signed score Δ_n , we permit abstention via the symmetric reject rule: output $X \rightarrow Y$ if $\Delta_n > \tau_n$, $Y \rightarrow X$ if $\Delta_n < -\tau_n$, and abstain otherwise. We set τ_n in *stability* mode (no labels): draw R subsamples (fraction 0.8) of the observed pair, compute $\Delta_n^{(r)}$ on each, and define

$$\tau_n := z_{1-\alpha/2} \widehat{\text{sd}}(\Delta_n^{(1)}, \dots, \Delta_n^{(R)}), \quad R = 50.$$

We run TRA-s and TRA-C with a Gaussian-copula confounding null, using $B = 500$ null bootstraps and $\alpha = 0.10$ for the two-sided significance/abstention test.

Metrics. We summarize performance by *coverage* $\text{Cov} = \frac{n_{\text{decided}}}{n}$, *decided accuracy* $\text{Acc}_d = \frac{n_{\text{correct}}}{n_{\text{decided}}}$, and the single scalar *directional risk* $\text{Risk} = (1 - \text{Acc}_d)\text{Cov} = \frac{n_{\text{wrong}}}{n}$, so a method is penalized either for wrong calls at high coverage or for excessive abstention, with Wilson-score confidence intervals for accuracy over decided pairs.

Baseline hyperparameter selection. To match our setting—unsupervised orientation from a single observational pair; we perform no label-based tuning on evaluation pairs. For unsupervised baselines (ANM/RESIT variants, IGCI, RECI, CDCI, bQCD/QCCD, COMIC, SLOPPY), we use authors’ defaults or *label-free* selection applied symmetrically in both directions: cross-validation for regression/conditional models, standard heuristics for independence tests (e.g., HSIC median bandwidth), and objective-based selection when available (e.g., COMIC ELBO). Any abstention thresholds (RECI/SLOPPY confidence rules, ANM test rejection, CDCI non-causal output) are fixed *a priori* or null calibrated, never tuned to ground-truth directions. Supervised transfer baselines (RCC, NCC) are trained/tuned only on external labeled/synthetic data and then frozen. For methods that permit a choice of regression backbone (e.g. TRA/TRA-s, RESIT, RECI), we standardize it to the same nonparametric regressor, smoothing splines (Wahba, 1990).

4.1. Synthetic Data

DGPs. We consider four synthetic additive-noise regimes, each with ground-truth direction $X \rightarrow Y$. In each regime we vary a single *stress* parameter and hold all others fixed: (i) *Cubic ANM (SNR sweep)*: $X \sim \mathcal{N}(0, 1)$, $Y = X^3 + \sigma_\varepsilon \epsilon$, $\epsilon \sim \mathcal{N}(0, 1)$; sweep σ_ε from low to high noise. (ii) *Near-linear ANM (nonlinearity sweep)*: $X \sim \mathcal{N}(0, 1)$, $Y = X + cX^3 + \sigma_\varepsilon \epsilon$, $\epsilon \sim \mathcal{N}(0, 1)$ with $\sigma_\varepsilon = 0.3$; sweep $c \downarrow 0$ toward the near-nonidentifiable linear limit. (iii) *Heteroscedastic cubic ANM (variance-drift sweep)*: $X \sim \mathcal{N}(0, 1)$, $Y = X^3 + \epsilon$ with $\epsilon = (\sigma_0 + \lambda|X|)\xi$, $\xi \sim \mathcal{N}(0, 1)$ and $\sigma_0 = 0.3$; sweep $\lambda \geq 0$ to increase heteroscedasticity. (iv) *Non-monotone sine ANM (noise sweep)*: $X \sim \text{Unif}[-1, 1]$, $Y = \sin(X) + \sigma_\varepsilon \epsilon$, $\epsilon \sim \mathcal{N}(0, 1)$; sweep σ_ε to increase noise under a non-monotone mechanism. For each scenario, we sweep sample size $n \in \{50, 100, 150, 250, 500, 1000, 1500, 2000\}$ and run $n_{\text{rep}} = 30$ independent Monte Carlo replicates per $(n, \text{parameter})$ setting. In each replicate we draw one dataset $\{(X_i, Y_i)\}_{i=1}^n$ and evaluate all methods on the same draw.

Figure 4 reports *directed risk* for all baselines across four ANM stress tests with ground-truth $X \rightarrow Y$, as we vary sample size n (vertical axis) and a scenario-specific stress parameter (horizontal axis). Most baselines are strongly *scenario dependent*: they excel in one panel yet fail in another, producing the high-risk bands across the atlas. In

contrast, the TRA family is consistently strong: raw TRA is best in the small-noise corner, while TRA-s stays low-risk in fixed-noise regimes where raw TRA cannot exploit reverse-cloud collapse. This matches the theory: Theorem 3.5 makes Δ_n informative as $\sigma_n \downarrow 0$, and Theorem 3.9 shows that smoothing ($\tilde{\Delta}_{0,n}$) restores separation at fixed noise by averaging reverse fluctuations at a mesoscopic scale.

In *cubic ANM (noise/SNR sweep)*, raw TRA improves rapidly as noise decreases, in line with Theorem 3.5: in the low-noise corner the reverse copula cloud becomes tube-like and MST merges fall below α_n , so Δ_n cleanly separates directions. As noise grows this collapse disappears and raw TRA degrades, whereas TRA-s stays stable across the sweep, consistent with Theorem 3.9. Several classical pipelines fail in stress-dependent bands, and supervised predictors (NCC/RCC/COMIC) show pronounced distribution-shift sensitivity with broad high-risk regions. In *near-linear ANM (nonlinearity sweep)*, identifiability weakens as the cubic perturbation vanishes. As expected, many baselines develop elevated risk bands as the decision signal collapses. Even in this corridor, TRA-s remains among the most reliable methods, highlighting that it is driven by forward-reverse residual *geometry* after copula standardization and smoothing, rather than by a single parametric asymmetry that must stay bounded away from zero. In *heteroscedastic cubic ANM (variance-drift sweep)*, increasing λ violates homoscedastic-noise assumptions and degrades several baselines. Methods that exploit richer conditional-distribution information (e.g., CDCI/bQCD) are more tolerant once n is large enough to estimate these quantities. TRA-s remains low-risk across λ and n , consistent with mesoscopic bin-averaging damping variance-driven fluctuations while preserving directional separation. Finally, in the *non-monotone sine ANM (noise sweep)*, the forward map is many-to-one, so reverse regression must mix multiple inverse branches. Supervised predictors again show pronounced instability across the grid, whereas TRA-s remains competitive and improves with n . In the *monotone* regimes (cubic and near-linear), the strong performance of TRA-s also supports the role of our forward-model regularity condition (Assumption 3.2), under which the reverse oracle cloud concentrates on a finite union of smooth strands as a noise vanishes.

Latent confounding setting (no true direction). To evaluate abstention under dependence-without-direction, we simulate *confounding-only* models driven by a latent Z . In the linear case, $Z \sim \mathcal{N}(0, 1)$, $X = Z + \varepsilon_X$, $Y = \gamma Z + \varepsilon_Y$, with $\varepsilon_X \sim \mathcal{N}(0, \sigma_X^2)$ and $\varepsilon_Y \sim \mathcal{N}(0, \sigma_Y^2)$ independent of Z ; we sweep γ . We also test a *nonlinear* confounded scenario by adding a symmetric cubic warp: $Z \sim \mathcal{N}(0, 1)$, $X = Z + aZ^3 + \varepsilon_X$, and $Y = bZ + aZ^3 + \varepsilon_Y$, with b fixed and a swept. Since neither $X \rightarrow Y$ nor $Y \rightarrow X$ holds, *directional accuracy is undefined* and we report cov-

erage (the fraction of non-abstained decisions). Figure 3 tracks coverage (with confidence intervals) as a function of the stress parameter (γ or a ; top row) and, after averaging over the stress sweep, as a function of sample size n (bottom row). Most direction-forcing baselines (RESIT, IGCI, CDCI, RCC, bQCD, SLOPPY) sustain near-unit coverage across parameters, i.e., they almost always output a direction despite the absence of a causal arrow. A partial exception is RECI: its mean coverage drops with n in parts of the sweep, plausibly because its score difference shrinks or destabilizes under symmetric confounding; but this abstention is uncalibrated and offers no controlled “no-direction” guarantee. In contrast, TRA-C calibrates score magnitude with a plug-in Gaussian-copula bootstrap under a confounding null and exhibits the intended reject behavior, abstaining rather than hallucinating an arrow in both the linear and nonlinear sweeps.

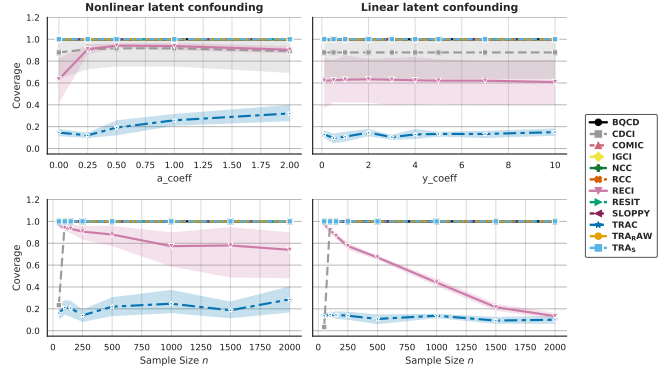


Figure 3. Evolution of coverage under (non)linear latent confounding as function of stress parameters (top) and sample size (bottom). Lower is better.

4.2. Real-world experiments

We benchmark on curated observational cause–effect datasets with unknown data-generating processes, where standard identifiability assumptions may fail, using the Tübingen Cause–Effect Pairs benchmark (Mooij et al., 2016) (108 labeled real-world pairs). For compatibility with common univariate baselines, we restrict to 30 pairs where both the annotated cause and effect are univariate. Figure 5 summarizes performance via *coverage*, *accuracy on decided*, and *directed risk* (penalizing both wrong calls and abstention), yielding two conclusions.

First, TRA variants give the best accuracy–coverage trade-off: TRA-C is deliberately conservative, attaining the highest decided accuracy and lowest directed risk overall, while TRA-s is the strongest high-coverage option, deciding on most pairs with (best/near-best) accuracy and the second-lowest risk. Second, competing families show the expected distribution-shift brittleness on real pairs: scalar-score baselines (RECI, RESIT, SLOPPY) and distributional criteria (CDCI, bQCD) achieve only moderate accuracy and higher

Topological Residual Asymmetry for Bivariate Causal Direction



Figure 4. Synthetic ANM atlas. Directed risk vs. sample size n and the scenario stress parameter. TRA-s is consistently low-risk across regimes; baselines show regime-specific failures.

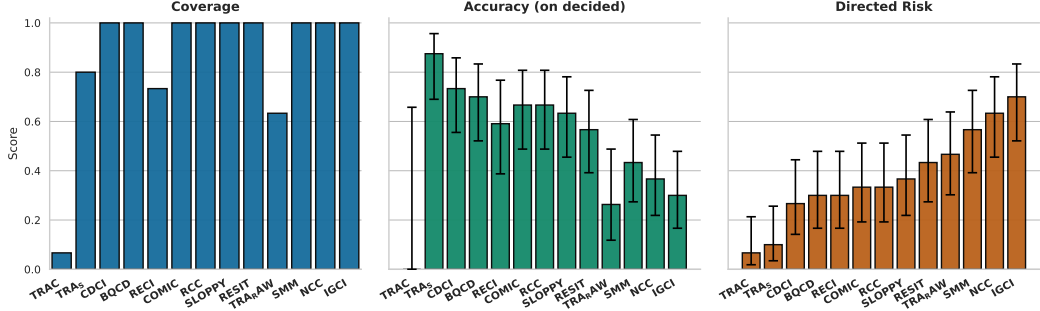


Figure 5. Results on Tübingen cause–effect pairs. Coverage, accuracy conditional on deciding, and directed risk for all methods.

risk than TRA-s, and supervised predictors are least reliable (NCC and IGCI incur the largest risks), consistent with sensitivity to heterogeneous real-world mechanisms and marginals. Finally, TRA-C’s low risk is not due to abstention alone—risk penalizes abstention—but to a reduction in wrong orientations that outweighs the abstention penalty; when coverage is the priority, TRA-s is the appropriate operating point.

Conclusion. We introduced *Topological Residual Asymmetry* (TRA), which infers causal direction from the copula-standardized geometry of cross-fitted regressor–residual clouds via Euclidean MST summary. We proved consistency in a triangular-array small-noise regime, showed that

mesoscopic binning (TRA-s) restores separation under fixed noise, and proposed TRA-C, a confounding-aware abstention rule calibrated by a Gaussian-copula null. Across synthetic stress tests and Tübingen pairs, TRA variants deliver the best accuracy–coverage tradeoff and lowest directed risk. Next steps include extending TRA to multivariate discovery by using local residual-asymmetry tests for edge orientation (Peters et al., 2017; Zheng et al., 2018), and leveraging limit theory for random geometric graphs/complexes to obtain calibrated uncertainty and higher-order topological summaries beyond MSTs (Penrose, 2003; Bobrowski & Kahle, 2018; Skraba & Yogeshwaran, 2022).

Impact Statement

This work advances methodology for causal direction inference from observational data by proposing a topological, abstention-capable criterion for bivariate additive-noise models. Potential positive impacts include more reliable orientation decisions, especially via abstention in ambiguous or confounded settings, which may reduce downstream harm from overconfident causal claims in scientific applications. At the same time, causal direction estimates can be misused or overinterpreted, particularly when applied outside the assumed regime or in high-stakes domains; our results therefore do not justify automated decision-making without domain expertise and careful validation. We expect no direct negative societal impact from releasing this method and provide abstention, calibration mechanisms, and confidence intervals intended to discourage unwarranted causal conclusions.

References

Blöbaum, P., Janzing, D., Washio, T., and Shimizu, S. Cause-effect inference by comparing regression errors. In *Proceedings of the 21st International Conference on Artificial Intelligence and Statistics (AISTATS)*, volume 84 of *Proceedings of Machine Learning Research*, pp. 1084–1092, 2018.

Bobrowski, O. and Kahle, M. Topology of random geometric complexes: A survey. *Journal of Applied and Computational Topology*, 1(3-4):331–364, 2018. doi: 10.1007/s41468-017-0010-0.

Camastra, F. Intrinsic dimension estimation: Advances and open problems. *Information Sciences*, 328:26–41, 2016. doi: 10.1016/j.ins.2015.12.012.

Cattaneo, M. D., Crump, R. K., Farrell, M. H., and Feng, Y. On binscatter. *American Economic Review*, 114(5): 1488–1514, 2024. doi: 10.1257/aer.20221576.

Chernozhukov, V., Chetverikov, D., Demirer, M., Duflo, E., Hansen, C., Newey, W., and Robins, J. Double/debiased machine learning for treatment and structural parameters. *The Econometrics Journal*, 21(1):C1–C68, 01 2018. ISSN 1368-4221. doi: 10.1111/ectj.12097. URL <https://doi.org/10.1111/ectj.12097>.

Chow, C. K. On optimum recognition error and reject tradeoff. *IEEE Transactions on Information Theory*, 16 (1):41–46, 1970. doi: 10.1109/TIT.1970.1054406.

Cohen-Steiner, D., Edelsbrunner, H., and Harer, J. Stability of persistence diagrams. *Discrete & Computational Geometry*, 37(1):103–120, 2007. doi: 10.1007/s00454-006-1276-5. URL <https://doi.org/10.1007/s00454-006-1276-5>.

Costa, J. A. and Hero, A. O. Geodesic entropic graphs for dimension and entropy estimation in manifold learning. *IEEE Transactions on Signal Processing*, 52(8):2210–2221, 2004a. doi: 10.1109/TSP.2004.831130.

Costa, J. A. and Hero, A. O. Geodesic entropic graphs for dimension and entropy estimation in manifold learning. *IEEE Transactions on Signal Processing*, 52(8):2210–2221, 2004b. doi: 10.1109/TSP.2004.831130.

Devroye, L. Laws of the iterated logarithm for order statistics of uniform spacings. *The Annals of Probability*, 9(4): 860–867, 1981. doi: 10.1214/aop/1176994472.

Duong, B. and Nguyen, T. Bivariate causal discovery via conditional divergence. In Schölkopf, B., Uhler, C., and Zhang, K. (eds.), *Proceedings of the First Conference on Causal Learning and Reasoning*, volume 177 of *Proceedings of Machine Learning Research*, pp. 236–252. PMLR, 2022. URL <https://proceedings.mlr.press/v177/duong22a.html>.

Edelsbrunner, H., Letscher, D., and Zomorodian, A. Topological persistence and simplification. *Discrete & Computational Geometry*, 28(4):511–533, 2002. doi: 10.1007/s00454-002-2885-2. URL <https://doi.org/10.1007/s00454-002-2885-2>.

El-Yaniv, R. and Wiener, Y. On the foundations of noise-free selective classification. *Journal of Machine Learning Research*, 11:1605–1641, 2010.

Fermanian, J. D., Radulović, D., and Wegkamp, M. Weak convergence of empirical copula processes. *Bernoulli*, 10 (5):847–860, 2004. doi: 10.3150/bj/1099579158.

Genest, C. and Rémillard, B. Validity of the parametric bootstrap for goodness-of-fit testing in semiparametric models. *Annales de l’Institut Henri Poincaré Probabilités et Statistiques*, 44(6):1096–1127, 2008. doi: 10.1214/07-AIHP148.

Ghrist, R. Barcodes: The persistent topology of data. *Proceedings of the National Academy of Sciences*, 105(1): 52–57, 2008. doi: 10.1073/pnas.0701744105.

Glymour, C., Zhang, K., and Spirtes, P. Review of causal discovery methods based on graphical models. *Frontiers in Genetics*, 10:524, 2019. doi: 10.3389/fgene.2019.00524.

Goudet, O., Kalainathan, D., Caillou, P., Guyon, I., Lopez-Paz, D., and Sebag, M. Causal generative neural networks. *arXiv preprint arXiv:1711.08936*, 2018. URL <https://arxiv.org/abs/1711.08936>. Version published at ICLR 2018 workshop.

Gower, J. C. and Ross, G. J. S. Minimum spanning trees and single linkage cluster analysis. *Journal of the Royal Statistical Society: Series C (Applied Statistics)*, 18(1): 54–64, 1969. doi: 10.2307/2346439. URL <https://doi.org/10.2307/2346439>.

Gretton, A., Bousquet, O., Smola, A. J., and Schölkopf, B. Measuring statistical dependence with hilbert–schmidt norms. *Journal of Machine Learning Research*, 6:2075–2129, 2005. URL <https://www.gatsby.ucl.ac.uk/~gretton/papers/GreBouSmoSch05.pdf>.

Györfi, L., Kohler, M., Krzyżak, A., and Walk, H. *A Distribution-Free Theory of Nonparametric Regression*. Springer, 2002. ISBN 978-0-387-95379-1.

Hoff, P. D. Extending the rank likelihood for semiparametric copula estimation. *The Annals of Applied Statistics*, 1(1): 265–283, 2007. doi: 10.1214/07-AOAS107.

Hoyer, P. O., Janzing, D., Mooij, J. M., Peters, J., and Schölkopf, B. Nonlinear causal discovery with additive noise models. In Koller, D., Schuurmans, D., Bengio, Y., and Bottou, L. (eds.), *Advances in Neural Information Processing Systems 21*, pp. 689–696. Curran Associates, Inc., 2009. URL <https://webdav.tuebingen.mpg.de/causality/NIPS2008-Hoyer.pdf>. Proceedings of NIPS 2008.

Janzing, D., Mooij, J., Zhang, K., Lemeire, J., Zscheischler, J., Daniušis, P., Steudel, B., and Schölkopf, B. Information-geometric approach to inferring causal directions (igci). *Artificial Intelligence*, 182–183:1–31, 2012. doi: 10.1016/j.artint.2012.01.002. URL <https://staff.fnwi.uva.nl/j.m.mooij/articles/ai2012.pdf>.

Kruskal, J. B. On the shortest spanning subtree of a graph and the traveling salesman problem. *Proceedings of the American Mathematical Society*, 7(1):48–50, 1956. doi: 10.1090/S0002-9939-1956-0078686-7.

Liu, H., Lafferty, J., and Wasserman, L. The nonparanormal: Semiparametric estimation of high dimensional undirected graphs. *Journal of Machine Learning Research*, 10(80):2295–2328, 2009.

Lopez-Paz, D., Muandet, K., and Recht, B. The randomized causation coefficient. *Journal of Machine Learning Research*, 16(1):2901–2907, 2015. URL <http://jmlr.org/papers/v16/lopez-paz15a.html>.

Lopez-Paz, D., Nishihara, R., Chintala, S., Scholkopf, B., and Bottou, L. Discovering causal signals in images. In *Proceedings of the IEEE Conference on Computer Vision and Pattern Recognition (CVPR)*, July 2017. URL https://openaccess.thecvf.com/content_cvpr_2017/html/Lopez-Paz_Discovering_Causal_CVPR_2017_paper.html.

Marx, A. and Vreeken, J. Identifiability of cause and effect using regularized regression. In *Proceedings of the 25th ACM SIGKDD International Conference on Knowledge Discovery and Data Mining (KDD)*, 2019.

Mitrović, J., Sejdinovic, D., and Teh, Y. W. Causal inference via kernel deviance measures. *arXiv preprint arXiv:1804.04622*, 2018.

Mooij, J. M., Peters, J., Janzing, D., Zscheischler, J., and Schölkopf, B. Distinguishing cause from effect using observational data: Methods and benchmarks. *Journal of Machine Learning Research*, 17(32):1–102, 2016.

Nelsen, R. B. *An Introduction to Copulas*. Springer Series in Statistics. Springer, New York, 2 edition, 2006.

Pearl, J. *Causality: Models, Reasoning, and Inference*. Cambridge University Press, Cambridge, UK, 2nd edition, 2009. ISBN 9780521895606. doi: 10.1017/CBO9780511803161.

Penrose, M. *Random Geometric Graphs*, volume 5 of *Oxford Studies in Probability*. Oxford University Press, 2003. ISBN 9780198506263.

Penrose, M. D. and Yukich, J. E. Laws of large numbers for nearest-neighbor distances and other geometric functionals. *The Annals of Applied Probability*, 19(3):972–994, 2009. URL <https://projecteuclid.org/euclid.aoap/1241497254>.

Peters, J., Mooij, J. M., Janzing, D., and Schölkopf, B. Causal discovery with continuous additive noise models. *Journal of Machine Learning Research*, 15:2009–2053, 2014. URL <https://www.jmlr.org/papers/volume15/peters14a/peters14a.pdf>.

Peters, J., Janzing, D., and Schölkopf, B. *Elements of Causal Inference: Foundations and Learning Algorithms*. Adaptive Computation and Machine Learning. The MIT Press, Cambridge, MA, USA, 2017. ISBN 9780262037310. URL <https://mitpress.mit.edu/9780262037310/elements-of-causal-inference/>.

Seo, C. and Yukich, J. E. A central limit theorem for the optimal transportation cost in high dimensions. *Advances in Applied Probability*, 32(3):579–597, 2000. doi: 10.1239/aap/1011994021.

Skraba, P. and Yogeshwaran, D. Central limit theorems for euclidean minimal spanning acycles. *Journal of*

Topology and Analysis, 14(4):933–975, 2022. doi: 10.1142/S1793525323500496. arXiv:2205.12348.

Spirites, P., Glymour, C., and Scheines, R. *Causation, Prediction, and Search*. The MIT Press, Cambridge, MA, USA, 2nd edition, 2001. ISBN 9780262527927.

Steele, J. M. Growth rates of euclidean minimal spanning trees with power weighted edges. *The Annals of Probability*, 1988.

Tagasovska, N., Chavez-Demoulin, V., and Vatter, T. Distinguishing cause from effect using quantiles: Bivariate quantile causal discovery. In *Proceedings of the 37th International Conference on Machine Learning*, volume 119 of *Proceedings of Machine Learning Research*, pp. 907–916. PMLR, 2020. URL <https://proceedings.mlr.press/v119/tagasovska20a.html>.

Tran, Q.-D., Duong, B., Nguyen, P., and Nguyen, T. Identifying causal direction via variational bayesian compression. *arXiv preprint arXiv:2505.07503*, 2025. doi: 10.48550/arXiv.2505.07503. URL <https://arxiv.org/abs/2505.07503>. Accepted at the 42nd International Conference on Machine Learning (ICML 2025).

Tukey, J. W. Curves as parameters, and touch estimation. In Neyman, J. (ed.), *Proceedings of the Fourth Berkeley Symposium on Mathematical Statistics and Probability, Volume 1: Contributions to the Theory of Statistics*, pp. 681–694. University of California Press, Berkeley, CA, 1961.

Varando, G., McConville, T., and Bühlmann, P. Pairwise causal discovery with support measure machines. *Applied Soft Computing*, 2024.

Vershynin, R. *High-Dimensional Probability: An Introduction with Applications in Data Science*. Cambridge University Press, 2018.

Wahba, G. *Spline Models for Observational Data*, volume 59 of *CBMS-NSF Regional Conference Series in Applied Mathematics*. SIAM, 1990. doi: 10.1137/1.9781611970128.

Wu, P. and Fukumizu, K. Causal mosaic: Cause-effect inference via nonlinear ica and ensemble method. In *Proceedings of the Twenty Third International Conference on Artificial Intelligence and Statistics*, volume 108 of *Proceedings of Machine Learning Research*, pp. 1157–1167. PMLR, 26–28 Aug 2020. URL <https://proceedings.mlr.press/v108/wu20b.html>.

Zhang, K., Peters, J., Janzing, D., and Schölkopf, B. Kernel-based conditional independence test and application in causal discovery. In *Proceedings of the Twenty-Eighth Conference on Uncertainty in Artificial Intelligence (UAI)*, 2012.

Zheng, X., Aragam, B., Ravikumar, P., and Xing, E. P. Dags with no tears: Continuous optimization for structure learning. In *Advances in Neural Information Processing Systems 31 (NeurIPS 2018)*, 2018. URL <https://arxiv.org/abs/1803.01422>. arXiv:1803.01422 [stat.ML].

A. Background

This appendix collects standard probabilistic and geometric notions used in the proofs.

A.1. Probability, laws, and stochastic order

Underlying probability space. All random objects are defined on a common probability space $(\Omega, \mathcal{F}, \mathbb{P})$. For a measurable map $Z : \Omega \rightarrow \mathbb{R}^2$, we write $\mathcal{L}(Z)$ for its distribution.

Definition A.1 (Law / pushforward). Let $Z : \Omega \rightarrow \mathbb{R}^2$ be measurable. The *law* of Z is the pushforward probability measure

$$\mathcal{L}(Z) := \mathbb{P} \circ Z^{-1} \in \mathcal{P}(\mathbb{R}^2).$$

Equivalently, for every bounded measurable $\varphi : \mathbb{R}^2 \rightarrow \mathbb{R}$,

$$\int_{\mathbb{R}^2} \varphi(z) \mathcal{L}(Z)(dz) = \mathbb{E}[\varphi(Z)].$$

Definition A.2 (Coupling). Let $\mu, \nu \in \mathcal{P}(\mathbb{R}^2)$. A *coupling* of (μ, ν) is a probability measure $\pi \in \mathcal{P}(\mathbb{R}^2 \times \mathbb{R}^2)$ with marginals μ and ν , i.e. for all Borel sets $A \subset \mathbb{R}^2$,

$$\pi(A \times \mathbb{R}^2) = \mu(A), \quad \pi(\mathbb{R}^2 \times A) = \nu(A).$$

Equivalently, a coupling can be realized as a pair of random vectors (U, V) on a single probability space such that $\mathcal{L}(U) = \mu$, $\mathcal{L}(V) = \nu$, and then $\pi = \mathcal{L}(U, V)$.

Stochastic order notation. For sequences of random variables (Z_n) and positive reals (a_n) , we use $O_{\mathbb{P}}$ and $o_{\mathbb{P}}$ in the standard sense.

Definition A.3 (Big- O and little- o in probability). We write $Z_n = O_{\mathbb{P}}(a_n)$ if $(|Z_n|/a_n)$ is bounded in probability, i.e. for every $\varepsilon > 0$ there exist $M < \infty$ and n_0 such that $\mathbb{P}(|Z_n| > Ma_n) \leq \varepsilon$ for all $n \geq n_0$. We write $Z_n = o_{\mathbb{P}}(a_n)$ if $Z_n/a_n \xrightarrow{\mathbb{P}} 0$, i.e. for every $\varepsilon > 0$, $\mathbb{P}(|Z_n| > \varepsilon a_n) \rightarrow 0$.

Remark A.4 (Basic algebra). If $Z_n = o_{\mathbb{P}}(a_n)$ then $Z_n = O_{\mathbb{P}}(a_n)$. If $Z_n = O_{\mathbb{P}}(a_n)$ and $W_n = O_{\mathbb{P}}(b_n)$, then $Z_n + W_n = O_{\mathbb{P}}(a_n + b_n)$ and $Z_n W_n = O_{\mathbb{P}}(a_n b_n)$.

A.2. Bounded-Lipschitz distance

We measure weak convergence of probability measures on \mathbb{R}^2 using the bounded-Lipschitz metric.

Definition A.5 (Bounded-Lipschitz metric). For $\mu, \nu \in \mathcal{P}(\mathbb{R}^2)$ and measurable $\varphi : \mathbb{R}^2 \rightarrow \mathbb{R}$, set $\|\varphi\|_{\infty} := \sup_{z \in \mathbb{R}^2} |\varphi(z)|$ and $\text{Lip}(\varphi) := \sup_{z \neq z'} |\varphi(z) - \varphi(z')|/\|z - z'\|_2$. Let

$$\text{BL}_1(\mathbb{R}^2) := \{\varphi : \|\varphi\|_{\infty} \leq 1, \text{Lip}(\varphi) \leq 1\}.$$

Define

$$d_{\text{BL}}(\mu, \nu) := \sup_{\varphi \in \text{BL}_1(\mathbb{R}^2)} \left| \int \varphi d\mu - \int \varphi d\nu \right|.$$

Remark A.6 (Coupling bound and finiteness). For any coupling (U, V) of (μ, ν) and any $\varphi \in \text{BL}_1(\mathbb{R}^2)$, $|\mathbb{E}[\varphi(U)] - \mathbb{E}[\varphi(V)]| \leq \mathbb{E}\|U - V\|_2$, hence

$$d_{\text{BL}}(\mu, \nu) \leq \mathbb{E}\|U - V\|_2.$$

Unlike W_1 , d_{BL} is finite for all probability measures since test functions are uniformly bounded.

A.3. Copulas and empirical copula coordinates

Copulas. Let (X, Y) have joint CDF $F_{X,Y}$ and marginal CDFs F_X, F_Y .

Definition A.7 (Bivariate copula). A *copula* is a CDF $C : [0, 1]^2 \rightarrow [0, 1]$ with uniform marginals. Equivalently, C is the joint CDF of some (U, V) with $U, V \sim \text{Unif}[0, 1]$.

Theorem A.8 (Sklar). *There exists a copula C such that $F_{X,Y}(x, y) = C(F_X(x), F_Y(y))$ for all x, y . If F_X and F_Y are continuous, then C is unique and $(F_X(X), F_Y(Y))$ has copula C .*

Pseudo-observations via ranks. Given a univariate sample W_1, \dots, W_n with continuous distribution, define

$$\text{rank}(W_i) := \#\{j : W_j \leq W_i\} \in \{1, \dots, n\}, \quad \widehat{U}_i := \frac{\text{rank}(W_i)}{n+1} \in \left(\frac{1}{n+1}, \frac{n}{n+1}\right),$$

where the $(n+1)$ scaling avoids the boundaries $\{0, 1\}$.

Definition A.9 (Empirical copula). Given a bivariate sample $(A_i, B_i)_{i=1}^n$ with continuous marginals, set $U_i^{(A)} := \text{rank}(A_i)/(n+1)$ and $U_i^{(B)} := \text{rank}(B_i)/(n+1)$, and define

$$C_n(u, v) := \frac{1}{n} \sum_{i=1}^n \mathbf{1}\{U_i^{(A)} \leq u, U_i^{(B)} \leq v\}, \quad (u, v) \in [0, 1]^2.$$

A.4. Distances between point clouds

Hausdorff distance. For nonempty $A \subset \mathbb{R}^2$ and $z \in \mathbb{R}^2$, let $d_2(z, A) := \inf_{a \in A} \|z - a\|_2$. For nonempty $A, B \subset \mathbb{R}^2$, define

$$d_H(A, B) := \max \left\{ \sup_{a \in A} d_2(a, B), \sup_{b \in B} d_2(b, A) \right\}.$$

If A, B are finite, the suprema are maxima and $d_H(A, B) < \infty$ automatically.

Gromov–Hausdorff distance. For compact metric spaces (X, d_X) and (Y, d_Y) ,

$$d_{\text{GH}}(X, Y) := \inf_{(Z, d_Z), \varphi, \psi} d_H^{(Z)}(\varphi(X), \psi(Y)),$$

where the infimum ranges over all metric spaces (Z, d_Z) and isometric embeddings $\varphi : X \hookrightarrow Z, \psi : Y \hookrightarrow Z$.

Remark A.10 (Ambient Hausdorff upper bound). If $A, B \subset \mathbb{R}^2$ are compact and are equipped with the induced Euclidean metric, then

$$d_{\text{GH}}(A, B) \leq d_H(A, B),$$

by taking $Z = \mathbb{R}^2$ and φ, ψ as inclusions.

A.5. Minimum spanning trees and H_0 persistence

In degree 0, persistent homology of a finite cloud is entirely about *connectivity* as the scale increases: connected components merge when edges appear, and each merge kills exactly one component. For the Vietoris–Rips filtration, the merge scales coincide with the edge lengths selected by Kruskal’s algorithm, hence with the edge lengths of a minimum spanning tree (MST). This identification lets us replace H_0 arguments by elementary graph/MST arguments throughout.

Weighted complete graph and MST. Let (S, d) be a finite metric space with $|S| = m$. Write $K(S)$ for the complete graph on vertex set S with edge weights $w(\{u, v\}) = d(u, v)$. A *spanning tree* is a connected acyclic subgraph on S with exactly $m - 1$ edges. A *minimum spanning tree (MST)* is a spanning tree minimizing the total weight $\sum_e w(e)$.

Theorem A.11 (H_0 persistence equals MST edge lengths). *Let (S, d) be a finite metric space with $|S| = m \geq 2$ and consider the Vietoris–Rips filtration with the convention that an edge $\{u, v\}$ appears at scale ϵ iff $d(u, v) \leq \epsilon$. Let T_{MST} be an MST of $(K(S), w)$ and list its edge lengths in nondecreasing order as $\ell_1 \leq \dots \leq \ell_{m-1}$. Then the multiset of finite death times in $\text{Dgm}_0(S)$ is exactly $\{\ell_j\}_{j=1}^{m-1}$; equivalently, $\text{Dgm}_0(S)$ has finite points $(0, \ell_1), \dots, (0, \ell_{m-1})$ and a single point $(0, \infty)$.*

Proof. For each $\epsilon \geq 0$, let G_ϵ be the Rips graph on S with edges $\{u, v\}$ such that $d(u, v) \leq \epsilon$. Connectivity of $\text{Rips}(S, \epsilon)$ is the same as connectivity of G_ϵ , since higher-dimensional simplices do not affect connected components. As ϵ increases, an H_0 class dies exactly when an edge is added between two previously disconnected components. Kruskal’s algorithm processes edges in increasing order and keeps precisely those that connect two distinct components; the accepted edges form an MST. Hence the $m - 1$ merge scales are $\ell_1, \dots, \ell_{m-1}$, and exactly one component persists forever. \square

Remark A.12 (Filtration parametrization and the factor 2). Some conventions build the filtration by growing closed balls of radius r and connecting points when balls intersect. Then $\{u, v\}$ appears when $r \geq \frac{1}{2}d(u, v)$, so death times are $\frac{1}{2}$ times the MST edge lengths. This is purely a choice of scale parameter.

Two MST facts used repeatedly. The following properties are standard and will be invoked without further comment.

Proposition A.13 (Cut property; uniqueness under distinct weights). *If all edge weights are distinct, then for any nontrivial cut $S = U \sqcup V$, the unique minimum-weight edge crossing the cut belongs to the MST. In particular, the MST is unique.*

Proof. If a spanning tree omits the lightest crossing edge, adding it creates a cycle containing another crossing edge of strictly larger weight; removing that heavier edge produces a spanning tree of smaller total weight, contradicting minimality. \square

Proposition A.14 (Minimum-bottleneck property). *Let T_{MST} be an MST and let T be any spanning tree on S . Then*

$$\max_{e \in T_{\text{MST}}} w(e) \leq \max_{e \in T} w(e).$$

Proof. Fix $\tau \geq 0$. If there exists a spanning tree using only edges of weight $\leq \tau$, then the graph induced by edges of weight $\leq \tau$ is connected, so Kruskal's algorithm can complete an MST without ever selecting an edge of weight $> \tau$. Taking $\tau = \max_{e \in T} w(e)$ yields the claim. \square

Practical translations used in our proofs. By Theorem A.11, statements about H_0 death times are statements about MST edge lengths. Two recurring maneuvers are: (i) to upper bound *all* death times, construct any spanning tree with controlled edge lengths and apply Proposition A.14 (e.g. a path along a discretized curve); and (ii) to control the number of short death times, use that every MST edge is some pair of points and hence can be bounded by counting pairs below a threshold.

H_0 as single-linkage clustering. The merge scales of single-linkage clustering are exactly the connectivity thresholds of G_ϵ , hence are encoded by the MST. This provides an equivalent, purely statistical interpretation of degree-0 persistence.

Stability for comparisons across clouds. When comparing clouds across small perturbations, we rely on standard stability of Vietoris–Rips persistence under Gromov–Hausdorff perturbations (and the ambient bound $d_{\text{GH}} \leq d_H$ from Remark A.10), which justifies controlling persistence-based summaries via Hausdorff-type estimates.

B. Proofs

B.1. Theorem 3.5

Auxiliary lemmas for Theorem 3.5. We collect here the four stability/separation ingredients used in the proof: (i) stability of copula standardization and approximation by rank maps (see Background, Section A.3); (ii) Lipschitz stability of the topological persistence functional in Hausdorff distance (see Background, Section A.4 for d_H); (iii) mesoscopic separation of 2D bulk clouds from 1D curve clouds; and (iv) a tube bound showing that reverse residuals concentrate near a finite union of C^1 curves.

Lemma B.1 (Copula stability and rank approximation). *Let (U, V) be a pair of real-valued random variables with continuous marginals and population copula map $T_{U,V}(u, v) := (F_U(u), F_V(v))$. Throughout, d_H denotes the Euclidean Hausdorff distance and d_{GH} the Gromov–Hausdorff distance (recalled in Background, Section A.4).*

(i) Bi-Lipschitzness on compact supports. Assume there exist compact intervals $I_U, I_V \subset \mathbb{R}$ such that $\mathbb{P}(U \in I_U) = \mathbb{P}(V \in I_V) = 1$ and $F_U, F_V \in C^1$ on I_U, I_V with

$$0 < c \leq F'_U(u) \leq C \quad (u \in I_U), \quad 0 < c \leq F'_V(v) \leq C \quad (v \in I_V).$$

Then for all $z, z' \in I_U \times I_V$,

$$c\|z - z'\|_2 \leq \|T_{U,V}(z) - T_{U,V}(z')\|_2 \leq C\|z - z'\|_2,$$

and for any finite nonempty clouds $A, B \subset I_U \times I_V$,

$$d_H(T_{U,V}(A), T_{U,V}(B)) \leq C d_H(A, B), \quad d_H(A, B) \leq c^{-1} d_H(T_{U,V}(A), T_{U,V}(B)).$$

(ii) Rank-copula approximation. Let $S_n = \{(U_i, V_i)\}_{i=1}^n$ be i.i.d. copies of (U, V) and define the coordinatewise rank map using the pseudo-observation convention from Background, Section A.3,

$$T_n(U_i, V_i) := \left(\frac{\text{rank}(U_i)}{n+1}, \frac{\text{rank}(V_i)}{n+1} \right) \quad (\text{ties broken deterministically}).$$

Then

$$\max_{1 \leq i \leq n} \|T_n(U_i, V_i) - T_{U,V}(U_i, V_i)\|_2 = O_{\mathbb{P}}(n^{-1/2}), \quad d_H(T_n(S_n), T_{U,V}(S_n)) = O_{\mathbb{P}}(n^{-1/2}).$$

(iii) **Two-cloud comparison.** For finite clouds $A_n, B_n \subset I_U \times I_V$, set

$$e_n(A_n) := d_H(T_n(A_n), T_{U,V}(A_n)), \quad e_n(B_n) := d_H(T_n(B_n), T_{U,V}(B_n)).$$

Then

$$d_H(T_n(A_n), T_n(B_n)) \leq e_n(A_n) + C d_H(A_n, B_n) + e_n(B_n), \quad d_{\text{GH}}(T_n(A_n), T_n(B_n)) \leq d_H(T_n(A_n), T_n(B_n)),$$

where the last inequality is the ambient Hausdorff upper bound recalled in Background, Section A.4.

Remark B.2 (Instantiation in our setting). In the proofs of Theorems 3.5 and 3.9, we apply Lemma B.1 with $(U, V) = (X, r^{(Y|X)})$ and $(U, V) = (Y_n, r^{(X|Y)})$. The compact-support and C^1 -CDF conditions required in part (i) hold on the relevant interior sets by Assumptions 3.2–3.3.

Lemma B.3 (Topological Persistence Stability). Let $n \geq 2$ and let $A, B \subset \mathbb{R}^2$ be clouds with $|A| = |B| = n$, equipped with the induced Euclidean metric. Then

$$|\text{TP}_{0,\Psi}^{[\alpha,\beta]}(A) - \text{TP}_{0,\Psi}^{[\alpha,\beta]}(B)| \leq 2 d_H(A, B),$$

where d_H is the Hausdorff distance (Background, Section A.4). Consequently, if $d_H(A_n, B_n) \rightarrow 0$, then $\text{TP}_{0,\Psi}^{[\alpha,\beta]}(A_n) - \text{TP}_{0,\Psi}^{[\alpha,\beta]}(B_n) \rightarrow 0$.

Lemma B.4 (Mesoscopic separation: 2D bulk vs. 1D curve). Let (α_n, β_n) satisfy the mesoscopic scale conditions of Equation (2). Assume moreover that the sampling model is either:

1. **(Bulk model)** $U_n = \{Z_i\}_{i=1}^n$ are i.i.d. on a rectangle $R \subset \mathbb{R}^2$ with density p bounded and bounded away from 0 on R ; or
2. **(Curve model)** $C_n = \{W_i\}_{i=1}^n$ are i.i.d. on a compact embedded C^1 curve $\Gamma \subset \mathbb{R}^2$ with respect to arc-length measure, with density q bounded and bounded away from 0 on Γ .

Then under (1),

$$\overline{\text{TP}}_0^{[\alpha_n, \beta_n]}(U_n) \xrightarrow{\mathbb{P}} 1.$$

And under (2),

$$\overline{\text{TP}}_0^{[\alpha_n, \beta_n]}(C_n) \xrightarrow{\mathbb{P}} 0.$$

Lemma B.5 (Reverse residuals lie in a thin tube (piecewise monotone case)). Fix a fold k and let $\{(X_i, Y_{n,i})\}_{i \in I_k}$ be i.i.d. from the small-noise ANM $Y_n = f(X) + \sigma_n \varepsilon$. Assume Assumptions 3.2 and 3.3. Assume moreover the reverse regression estimator satisfies the uniform-on-test-points bound in Assumption 3.4 (with $\delta_n^{(k)} = o_{\mathbb{P}}(1)$), and let $\omega(\cdot)$ denote the modulus of continuity of m_n on J_{η} from Assumption 3.3.

For each monotonicity interval I_j in Assumption 3.2, let $h_j : f(I_j) \rightarrow I_j$ be the inverse branch and set $J_{\eta,j} := J_{\eta} \cap f(I_j)$. Define the (deterministic) union-of-branches center set

$$\Gamma_{n,\eta} := \bigcup_{j=1}^J \Gamma_{n,\eta}^{(j)}, \quad \Gamma_{n,\eta}^{(j)} := \{(y, h_j(y) - m_n(y)) : y \in J_{\eta,j}\}.$$

Define the restricted reverse residual cloud

$$\mathcal{R}_{X|Y,k,\eta}^{(n)} := \{(Y_{n,i}, X_i - \widehat{g}_n^{(-k)}(Y_{n,i})) : i \in I_k, Y_{n,i} \in J_{\eta}\}.$$

Let $j(i) \in \{1, \dots, J\}$ be the branch index such that $X_i \in I_{j(i)}$. For each j , define

$$I_{k,j} := \{i \in I_k : j(i) = j, Y_{n,i} \in J_{\eta,j}\}, \quad \Delta_{n,\eta}^{(j)} := \sup_{y \in J_{\eta,j}} \min_{i \in I_{k,j}} |y - Y_{n,i}| \quad (\min \emptyset := +\infty).$$

On the event $\mathcal{E}_n := \{\forall j \text{ with } |J_{\eta,j}| > 0 : I_{k,j} \neq \emptyset\}$,

$$d_H(\mathcal{R}_{X|Y,k,\eta}^{(n)}, \Gamma_{n,\eta}) \leq \max_{1 \leq j \leq J} \left[\frac{\sigma_n}{c_f} \max_{i \in I_{k,j}} |\varepsilon_i| + \delta_n^{(k)} + \left(1 + \frac{1}{c_f}\right) \Delta_{n,\eta}^{(j)} + \omega(\Delta_{n,\eta}^{(j)}) \right],$$

where d_H is the Hausdorff distance (Background, Section A.4) and c_f is the uniform slope lower bound from Assumption 3.2. Moreover, under the branchwise lower-density condition in Assumption 3.3 (away from turning values), $\mathbb{P}(\mathcal{E}_n) \rightarrow 1$ and, for each fixed j ,

$$\Delta_{n,\eta}^{(j)} = O_{\mathbb{P}}\left(\frac{\log n}{n}\right).$$

In particular, under Assumption 3.4(iii) and $\frac{\log n}{n} = o(\alpha_n)$ together with $\delta_n^{(k)} = o_{\mathbb{P}}(\alpha_n)$,

$$d_H(\mathcal{R}_{X|Y,k,\eta}^{(n)}, \Gamma_{n,\eta}) = o_{\mathbb{P}}(\alpha_n).$$

Proof of Theorem 3.5.

Proof. Fix the mesoscopic window $\alpha_n = \kappa n^{-2/3}$ and $\beta_n = c_{\beta} \alpha_n$.

Proof strategy. We argue first in an *oracle copula world*, i.e. copula standardization is performed by population CDFs (Background, Section A.3). In the true direction this produces a 2D bulk cloud in $(0, 1)^2$, forcing $\overline{\text{TP}}_0^{[\alpha_n, \beta_n]} \rightarrow 1$ by Lemma B.4. In the reverse direction the residual cloud lies in an $o_{\mathbb{P}}(\alpha_n)$ -tube around a finite union of C^1 curves, forcing $\overline{\text{TP}}_0^{[\alpha_n, \beta_n]} \rightarrow 0$ again by Lemma B.4. Finally, we transfer from oracle copulas to rank copulas using Lemma B.1 together with Hausdorff stability of TP_0 (Lemma B.3), where d_H is as in Background, Section A.4.

Step 1 (oracle true direction): bulk $\Rightarrow \overline{\text{TP}} \rightarrow 1$. In the true direction, $r_{i,\circ}^{(Y|X)} = Y_{n,i} - f(X_i) = \sigma_n \varepsilon_i$ with $\varepsilon_i \perp\!\!\!\perp X_i$. Hence the population copula map

$$T_{\circ}^{\text{true}}(x, r) := (F_X(x), F_{\sigma_n \varepsilon}(r)) = (F_X(x), F_{\varepsilon}(r/\sigma_n))$$

sends $(X_i, r_{i,\circ}^{(Y|X)})$ to i.i.d. $\text{Unif}((0, 1)^2)$ points (Background, Section A.3). Therefore, by Lemma B.4,

$$\overline{\text{TP}}_0^{[\alpha_n, \beta_n]}(\widetilde{\mathcal{R}}_{\circ, Y|X}^{(n)}) \xrightarrow{\mathbb{P}} 1.$$

Step 2 (oracle reverse direction): tube around curves $\Rightarrow \overline{\text{TP}} \rightarrow 0$. Fix a fold k and the interior set $J_{\eta} \Subset f(I) \setminus \mathcal{V}$ from Assumption 3.3. By Lemma B.5 and Assumption 3.4,

$$d_H(\mathcal{R}_{X|Y,k,\eta}^{(n)}, \Gamma_{n,\eta}) = o_{\mathbb{P}}(\alpha_n).$$

Let T_{\circ}^{rev} denote the population copula map for the reverse pair $(Y_n, X - m_n(Y_n))$. On J_{η} turning values are excluded, so T_{\circ}^{rev} is bi-Lipschitz on the relevant compact region, and Lemma B.1(i) gives

$$d_H\left(T_{\circ}^{\text{rev}}(\mathcal{R}_{X|Y,k,\eta}^{(n)}), T_{\circ}^{\text{rev}}(\Gamma_{n,\eta})\right) = o_{\mathbb{P}}(\alpha_n).$$

The set $T_{\circ}^{\text{rev}}(\Gamma_{n,\eta})$ is a finite union of compact embedded C^1 curves in $(0, 1)^2$. Writing $C_n^{(j)}$ for the oracle points on the j -th component after copula standardization, each $C_n^{(j)}$ is i.i.d. on that curve with density bounded and bounded away from 0 with respect to arc-length, hence Lemma B.4 yields $\overline{\text{TP}}_0^{[\alpha_n, \beta_n]}(C_n^{(j)}) \xrightarrow{\mathbb{P}} 0$ for each j . Since the MST on the full union consists of the within-component MSTs plus at most $(J - 1)$ connecting edges, and each connecting edge contributes at most $1/(n - 1)$ to the normalized sum, we obtain

$$\overline{\text{TP}}_0^{[\alpha_n, \beta_n]}(T_{\circ}^{\text{rev}}(\Gamma_{n,\eta}^{\text{grid}})) = \sum_{j=1}^J \frac{|C_n^{(j)}| - 1}{n - 1} \overline{\text{TP}}_0^{[\alpha_n, \beta_n]}(C_n^{(j)}) + O\left(\frac{1}{n}\right) \xrightarrow{\mathbb{P}} 0.$$

Combining with the $o_{\mathbb{P}}(\alpha_n)$ Hausdorff tube bound and Lemma B.3 yields

$$\overline{\text{TP}}_0^{[\alpha_n, \beta_n]}(\widetilde{\mathcal{R}}_{\circ, X|Y}^{(n)}) \xrightarrow{\mathbb{P}} 0.$$

Step 3 (transfer oracle → ranks): rank-copula clouds inherit the limits. We now replace oracle copula standardization by empirical rank-copula standardization (Background, Section A.3).

True direction. Lemma B.1(ii) applied to $(X, r_{\circ}^{(Y|X)})$ gives

$$d_H\left(T_n(\mathcal{R}_{\circ,Y|X}^{(n)}), T_{\circ}^{\text{true}}(\mathcal{R}_{\circ,Y|X}^{(n)})\right) = O_{\mathbb{P}}(n^{-1/2}).$$

By Lemma B.3, the corresponding values of $\overline{\text{TP}}_0^{[\alpha_n, \beta_n]}$ differ by $o_{\mathbb{P}}(1)$, hence

$$\overline{\text{TP}}_0^{[\alpha_n, \beta_n]}(\tilde{\mathcal{R}}_{Y|X}^{(n)}) \xrightarrow{\mathbb{P}} 1.$$

Reverse direction. Applying Lemma B.1(ii) to the reverse pair and again using Lemma B.3 yields the analogous oracle-to-rank transfer, hence

$$\overline{\text{TP}}_0^{[\alpha_n, \beta_n]}(\tilde{\mathcal{R}}_{X|Y}^{(n)}) \xrightarrow{\mathbb{P}} 0.$$

Step 4 (decision statistic): $\Delta_n \rightarrow 1$ and vanishing abstention. Steps 1–3 give

$$\overline{\text{TP}}_0^{[\alpha_n, \beta_n]}(\tilde{\mathcal{R}}_{Y|X}^{(n)}) \xrightarrow{\mathbb{P}} 1, \quad \overline{\text{TP}}_0^{[\alpha_n, \beta_n]}(\tilde{\mathcal{R}}_{X|Y}^{(n)}) \xrightarrow{\mathbb{P}} 0,$$

hence $\Delta_n \xrightarrow{\mathbb{P}} 1$. If $\tau_n \downarrow 0$, then

$$\mathbb{P}(\widehat{\text{dir}}_n = X \rightarrow Y) \geq \mathbb{P}(\Delta_n > \tau_n) \rightarrow 1, \quad \mathbb{P}(\text{abstain}) = \mathbb{P}(|\Delta_n| \leq \tau_n) \leq \mathbb{P}(\Delta_n \leq \tau_n) \rightarrow 0,$$

which completes the proof. \square

B.1.1. PROOF OF LEMMAS

Proof of Lemma B.1. Throughout write $T := T_{U,V}$ and let I_U, I_V be as in the statement.

Part (i): bi-Lipschitzness and Hausdorff control.

Step 1: coordinatewise Lipschitz bounds. Fix $u, u' \in I_U$. By the mean value theorem there exists ξ between u and u' such that $F_U(u) - F_U(u') = F'_U(\xi)(u - u')$. Using $c \leq F'_U \leq C$ on I_U gives $c|u - u'| \leq |F_U(u) - F_U(u')| \leq C|u - u'|$. The same argument yields, for all $v, v' \in I_V$, $c|v - v'| \leq |F_V(v) - F_V(v')| \leq C|v - v'|$.

Step 2: bi-Lipschitzness of the copula map on $I_U \times I_V$. For $z = (u, v)$ and $z' = (u', v')$ in $I_U \times I_V$,

$$\|T(z) - T(z')\|_2^2 = |F_U(u) - F_U(u')|^2 + |F_V(v) - F_V(v')|^2 \leq C^2(|u - u'|^2 + |v - v'|^2) = C^2\|z - z'\|_2^2,$$

and similarly $\|T(z) - T(z')\|_2^2 \geq c^2\|z - z'\|_2^2$. Taking square roots gives

$$c\|z - z'\|_2 \leq \|T(z) - T(z')\|_2 \leq C\|z - z'\|_2.$$

Step 3: Hausdorff control under Lipschitz maps. Recall the definition of d_H and the point-to-set distance $d_2(\cdot, \cdot)$ from Background, Section A.4. If Φ is L -Lipschitz, then for any nonempty A, B ,

$$\sup_{a \in A} d_2(\Phi(a), \Phi(B)) = \sup_{a \in A} \inf_{b \in B} \|\Phi(a) - \Phi(b)\|_2 \leq \sup_{a \in A} \inf_{b \in B} L\|a - b\|_2 \leq L \sup_{a \in A} d_2(a, B),$$

and symmetrically $\sup_{b \in B} d_2(\Phi(b), \Phi(A)) \leq L \sup_{b \in B} d_2(b, A)$, hence $d_H(\Phi(A), \Phi(B)) \leq L d_H(A, B)$. Applying this with $\Phi = T$ (which is C -Lipschitz by Step 2) yields

$$d_H(T(A), T(B)) \leq C d_H(A, B).$$

Step 4: reverse Hausdorff bound via the inverse map. Since $F'_U \geq c > 0$ on I_U , F_U is strictly increasing on I_U , hence injective there; likewise F_V on I_V . Thus T is injective on $I_U \times I_V$ and admits an inverse $T^{-1} : T(I_U \times I_V) \rightarrow I_U \times I_V$. Moreover Step 2 implies T^{-1} is $(1/c)$ -Lipschitz on its domain: if $u = T(z)$ and $u' = T(z')$, then

$$\|T^{-1}(u) - T^{-1}(u')\|_2 = \|z - z'\|_2 \leq \frac{1}{c} \|T(z) - T(z')\|_2 = \frac{1}{c} \|u - u'\|_2.$$

Applying the same Hausdorff-Lipschitz implication (from the definition of d_H) to $\Phi = T^{-1}$ gives

$$d_H(A, B) \leq \frac{1}{c} d_H(T(A), T(B)),$$

completing part (i).

Part (ii): rank-copula approximation on an i.i.d. sample. Let $S_n = \{(U_i, V_i)\}_{i=1}^n$ be i.i.d. copies of (U, V) , with continuous marginals. Then $\mathbb{P}(U_i = U_j \text{ for some } i \neq j) = 0$ and similarly for (V_i) , so ranks are well-defined a.s.

Let $\widehat{F}_{U,n}(t) := \frac{1}{n} \sum_{j=1}^n \mathbf{1}\{U_j \leq t\}$ and define $\widehat{F}_{V,n}$ analogously. On the no-ties event, $\widehat{F}_{U,n}(U_i) = \text{rank}(U_i)/n$ and $\widehat{F}_{V,n}(V_i) = \text{rank}(V_i)/n$. Write

$$T_n(U_i, V_i) = \left(\frac{\text{rank}(U_i)}{n+1}, \frac{\text{rank}(V_i)}{n+1} \right) =: (U_i^{(n)}, V_i^{(n)}).$$

Step 1: reduce to sup-norm empirical CDF errors. For each i ,

$$|U_i^{(n)} - \widehat{F}_{U,n}(U_i)| = \text{rank}(U_i) \left| \frac{1}{n+1} - \frac{1}{n} \right| \leq \frac{1}{n+1},$$

and hence

$$|U_i^{(n)} - F_U(U_i)| \leq \frac{1}{n+1} + \sup_{t \in \mathbb{R}} |\widehat{F}_{U,n}(t) - F_U(t)|.$$

Define $\Delta_{U,n} := \sup_t |\widehat{F}_{U,n}(t) - F_U(t)|$ and $\Delta_{V,n}$ similarly. Then for each i ,

$$\|T_n(U_i, V_i) - T(U_i, V_i)\|_2 \leq |U_i^{(n)} - F_U(U_i)| + |V_i^{(n)} - F_V(V_i)| \leq \Delta_{U,n} + \Delta_{V,n} + \frac{2}{n+1}.$$

Taking $\max_{1 \leq i \leq n}$ yields

$$\max_{1 \leq i \leq n} \|T_n(U_i, V_i) - T(U_i, V_i)\|_2 \leq \Delta_{U,n} + \Delta_{V,n} + \frac{2}{n+1}.$$

Step 2: apply DKW–Massart. By the DKW–Massart inequality, $\Delta_{U,n} = O_{\mathbb{P}}(n^{-1/2})$ and $\Delta_{V,n} = O_{\mathbb{P}}(n^{-1/2})$, while $\frac{2}{n+1} = O(n^{-1})$ deterministically. Therefore,

$$\max_{1 \leq i \leq n} \|T_n(U_i, V_i) - T(U_i, V_i)\|_2 = O_{\mathbb{P}}(n^{-1/2}).$$

Step 3: Hausdorff bound between the two standardized clouds. Let $a_i := T_n(U_i, V_i)$ and $b_i := T(U_i, V_i)$, so that $T_n(S_n) = \{a_i\}_{i=1}^n$ and $T(S_n) = \{b_i\}_{i=1}^n$. Using the point-to-set distance $d_2(\cdot, \cdot)$ from Background, Section A.4, for each i we have $d_2(a_i, T(S_n)) \leq \|a_i - b_i\|_2$, hence $\sup_{a \in T_n(S_n)} d_2(a, T(S_n)) \leq \max_i \|a_i - b_i\|_2$, and similarly with the roles swapped. Therefore,

$$d_H(T_n(S_n), T(S_n)) \leq \max_{1 \leq i \leq n} \|a_i - b_i\|_2 = O_{\mathbb{P}}(n^{-1/2}),$$

completing part (ii).

Part (iii): two-cloud comparison and d_{GH} bound. For finite clouds $A_n, B_n \subset I_U \times I_V$, the triangle inequality for d_H gives

$$d_H(T_n(A_n), T_n(B_n)) \leq d_H(T_n(A_n), T(A_n)) + d_H(T(A_n), T(B_n)) + d_H(T(B_n), T_n(B_n)).$$

The first and third terms are $e_n(A_n)$ and $e_n(B_n)$ by definition, and the middle term is bounded by $C d_H(A_n, B_n)$ by part (i), proving the stated deterministic inequality.

For the Gromov–Hausdorff bound, we invoke the ambient Hausdorff upper bound from Background, Remark A.10 (i.e. $d_{\text{GH}}(\mathcal{X}, \mathcal{Y}) \leq d_H(\mathcal{X}, \mathcal{Y})$ when \mathcal{X}, \mathcal{Y} are subsets of a common ambient metric space with induced metrics). Since $T_n(A_n), T_n(B_n) \subset (\mathbb{R}^2, \|\cdot\|_2)$,

$$d_{\text{GH}}(T_n(A_n), T_n(B_n)) \leq d_H(T_n(A_n), T_n(B_n)).$$

This completes the proof. \square

Proof of Lemma B.3. Let $A, B \subset \mathbb{R}^2$ be clouds with $|A| = |B| = m \geq 2$. Write

$$\text{Dgm}_0(A) = \{(0, \epsilon_j(A))\}_{j=1}^{m-1}, \quad \text{Dgm}_0(B) = \{(0, \epsilon_j(B))\}_{j=1}^{m-1},$$

where $\epsilon_j(\cdot)$ are the finite H_0 death times.

Step 1: bottleneck stability in the ambient space. By the stability of Vietoris–Rips persistence under d_{GH} ,

$$d_B(\text{Dgm}_0(A), \text{Dgm}_0(B)) \leq 2 d_{\text{GH}}(A, B).$$

Since $A, B \subset (\mathbb{R}^2, \|\cdot\|_2)$ with induced metrics, the ambient Hausdorff upper bound for d_{GH} (Background, Remark A.10) yields $d_{\text{GH}}(A, B) \leq d_H(A, B)$. Therefore,

$$d_B(\text{Dgm}_0(A), \text{Dgm}_0(B)) \leq 2 d_H(A, B).$$

Step 2: match H_0 deaths under the bottleneck distance. All births in H_0 are equal to 0, so d_B reduces to matching death times. Concretely, by the definition of d_B there exists a bijection $\pi : \{1, \dots, m-1\} \rightarrow \{1, \dots, m-1\}$ such that

$$\max_{1 \leq j \leq m-1} |\epsilon_j(A) - \epsilon_{\pi(j)}(B)| \leq d_B(\text{Dgm}_0(A), \text{Dgm}_0(B)).$$

Step 3: push the matching through the Lipschitz test function. Since $\Psi_{\alpha, \beta}$ is 1-Lipschitz, for each j ,

$$|\Psi_{\alpha, \beta}(\epsilon_j(A)) - \Psi_{\alpha, \beta}(\epsilon_{\pi(j)}(B))| \leq |\epsilon_j(A) - \epsilon_{\pi(j)}(B)|.$$

Averaging and using $\frac{1}{m-1} \sum_j |\epsilon_j(A)| \leq \max_j |\epsilon_j(A)|$ gives

$$\begin{aligned} |\text{TP}_{0, \Psi}^{[\alpha, \beta]}(A) - \text{TP}_{0, \Psi}^{[\alpha, \beta]}(B)| &= \left| \frac{1}{m-1} \sum_{j=1}^{m-1} (\Psi_{\alpha, \beta}(\epsilon_j(A)) - \Psi_{\alpha, \beta}(\epsilon_{\pi(j)}(B))) \right| \\ &\leq \frac{1}{m-1} \sum_{j=1}^{m-1} |\Psi_{\alpha, \beta}(\epsilon_j(A)) - \Psi_{\alpha, \beta}(\epsilon_{\pi(j)}(B))| \\ &\leq \max_{1 \leq j \leq m-1} |\epsilon_j(A) - \epsilon_{\pi(j)}(B)| \\ &\leq d_B(\text{Dgm}_0(A), \text{Dgm}_0(B)) \\ &\leq 2 d_H(A, B), \end{aligned}$$

which proves the claimed stability inequality.

Convergence consequence. If $d_H(A_n, B_n) \rightarrow 0$, then the inequality implies $|\text{TP}_{0, \Psi}^{[\alpha, \beta]}(A_n) - \text{TP}_{0, \Psi}^{[\alpha, \beta]}(B_n)| \rightarrow 0$. \square

Proof of Lemma B.4. Fix $m \geq 2$ and abbreviate $\alpha := \alpha_m, \beta := \beta_m$. Recall

$$\Psi_{\alpha, \beta}(t) = (\min\{t, \beta\} - \alpha)_+, \quad w_{\alpha, \beta}(t) := \frac{1}{\beta - \alpha} \Psi_{\alpha, \beta}(t) \in [0, 1],$$

so that $w_{\alpha, \beta}(t) = 1$ for $t \geq \beta$ and $w_{\alpha, \beta}(t) = 0$ for $t \leq \alpha$.

Part (a): bulk model $\Rightarrow \overline{\text{TP}}_0^{[\alpha_m, \beta_m]}(U_m) \rightarrow 1$. Let $U_m = \{Z_i\}_{i=1}^m$ with Z_i i.i.d. on a rectangle $R \subset \mathbb{R}^2$ and density p satisfying $0 < p(z) \leq p_{\max} < \infty$ on R .

Step A1 (deficit bound via counting short MST edges). Let $\{\varepsilon_j(S)\}_{j=1}^{m-1}$ denote the Euclidean MST edge lengths of a cloud S (equivalently, the finite H_0 death times under the Rips filtration; see Background, Theorem A.11). Define

$$N_{<\beta}(S) := \#\{j \in \{1, \dots, m-1\} : \varepsilon_j(S) < \beta\}.$$

Since $w_{\alpha, \beta}(\varepsilon_j) = 1$ for $\varepsilon_j \geq \beta$ and $w_{\alpha, \beta}(\varepsilon_j) \geq 0$ always,

$$\sum_{j=1}^{m-1} w_{\alpha, \beta}(\varepsilon_j(S)) \geq \sum_{j: \varepsilon_j(S) \geq \beta} 1 = (m-1) - N_{<\beta}(S).$$

Dividing by $m-1$ yields the deficit bound

$$0 \leq 1 - \overline{\text{TP}}_0^{[\alpha, \beta]}(S) \leq \frac{N_{<\beta}(S)}{m-1}. \quad (7)$$

Thus it suffices to show $N_{<\beta}(U_m) = o_{\mathbb{P}}(m)$.

Step A2 (short MST edges are controlled by close pairs). Let

$$P_{<\beta}(S) := \#\{\{u, v\} \subset S : \|u - v\|_2 < \beta\}$$

be the number of unordered pairs at Euclidean distance $< \beta$. Any MST edge of length $< \beta$ contributes such a pair, hence

$$N_{<\beta}(S) \leq P_{<\beta}(S).$$

It therefore suffices to prove $P_{<\beta}(U_m) = o_{\mathbb{P}}(m)$.

Step A3 (first moment bound for close pairs). Expanding as a sum of indicators,

$$P_{<\beta}(U_m) = \sum_{1 \leq i < j \leq m} \mathbf{1}\{\|Z_i - Z_j\|_2 < \beta\}.$$

Taking expectations and using identical distribution of pairs,

$$\mathbb{E}[P_{<\beta}(U_m)] = \binom{m}{2} \mathbb{P}(\|Z - Z'\|_2 < \beta),$$

where Z, Z' are i.i.d. with density p . Moreover,

$$\begin{aligned} \mathbb{P}(\|Z - Z'\|_2 < \beta) &= \int_R \int_R \mathbf{1}\{\|z - z'\|_2 < \beta\} p(z)p(z') dz' dz \\ &\leq p_{\max}^2 \int_R \text{Leb}(B(z, \beta) \cap R) dz \\ &\leq p_{\max}^2 \text{Leb}(R) \pi \beta^2. \end{aligned}$$

Consequently,

$$\mathbb{E}[P_{<\beta}(U_m)] \lesssim m^2 \beta^2.$$

Step A4 (Markov $\Rightarrow P_{<\beta}(U_m) = o_{\mathbb{P}}(m)$). By Markov's inequality, for any $\eta > 0$,

$$\mathbb{P}\left(\frac{P_{<\beta}(U_m)}{m} > \eta\right) \leq \frac{\mathbb{E}[P_{<\beta}(U_m)]}{\eta m} \lesssim \frac{m\beta^2}{\eta}.$$

Under the scale condition $m\beta^2 \rightarrow 0$, the right-hand side tends to 0, hence

$$\frac{P_{<\beta}(U_m)}{m} \xrightarrow{\mathbb{P}} 0, \quad \text{so} \quad P_{<\beta}(U_m) = o_{\mathbb{P}}(m).$$

Therefore $N_{<\beta}(U_m) \leq P_{<\beta}(U_m) = o_{\mathbb{P}}(m)$ as well.

Step A5 (finish). Plugging into (7) gives

$$0 \leq 1 - \overline{\text{TP}}_0^{[\alpha_m, \beta_m]}(U_m) \leq \frac{N_{<\beta_m}(U_m)}{m-1} \xrightarrow{\mathbb{P}} 0,$$

and hence $\overline{\text{TP}}_0^{[\alpha_m, \beta_m]}(U_m) \xrightarrow{\mathbb{P}} 1$.

Remark. Part (a) only uses the condition $m\beta_m^2 \rightarrow 0$.

Part (b): curve model $\Rightarrow \overline{\text{TP}}_0^{[\alpha_m, \beta_m]}(C_m) \rightarrow 0$. Assume now $C_m = \{W_i\}_{i=1}^m$ are i.i.d. on a compact embedded C^1 curve $\Gamma \subset \mathbb{R}^2$ with respect to arclength, with density q satisfying $0 < q_{\min} \leq q \leq q_{\max} < \infty$.

Step B1 (parametrization and a cheap spanning tree). Let $L := \text{length}(\Gamma)$ and fix an injective C^1 unit-speed parametrization $\gamma : [0, L] \rightarrow \mathbb{R}^2$ with $\|\gamma'(s)\|_2 = 1$ and $\Gamma = \gamma([0, L])$. Let $S_i \in [0, L]$ be the i.i.d. parameters with density q and set $W_i := \gamma(S_i)$. Write the order statistics $S_{(1)} \leq \dots \leq S_{(m)}$ and spacings

$$\Delta_i := S_{(i+1)} - S_{(i)} \quad (1 \leq i \leq m-1), \quad \Delta_{\max} := \max_{1 \leq i \leq m-1} \Delta_i, \quad W_{(i)} := \gamma(S_{(i)}).$$

Since γ is unit-speed, it is 1-Lipschitz: for $0 \leq s \leq t \leq L$,

$$\|\gamma(t) - \gamma(s)\|_2 \leq \int_s^t \|\gamma'(u)\|_2 du = t - s.$$

Therefore, for each i ,

$$\|W_{(i+1)} - W_{(i)}\|_2 \leq S_{(i+1)} - S_{(i)} = \Delta_i \leq \Delta_{\max}.$$

Consider the path spanning tree connecting consecutive points $W_{(i)} - W_{(i+1)}$ for $i = 1, \dots, m-1$. This is a spanning tree whose maximum edge length is at most Δ_{\max} .

Step B2 (MST bottleneck property). By the minimum-bottleneck property of MSTs (Background, Proposition A.14),

$$\max_{1 \leq j \leq m-1} \varepsilon_j(C_m) \leq \Delta_{\max},$$

where $\{\varepsilon_j(C_m)\}$ are the MST edge lengths of C_m .

Step B3 (if $\Delta_{\max} < \alpha$, then the windowed score is zero). On the event $\{\Delta_{\max} < \alpha\}$ we have $\varepsilon_j(C_m) < \alpha$ for all j , hence $\Psi_{\alpha, \beta}(\varepsilon_j(C_m)) = 0$ for all j (since $t \leq \alpha \Rightarrow \Psi_{\alpha, \beta}(t) = 0$). Therefore

$$\overline{\text{TP}}_0^{[\alpha, \beta]}(C_m) = 0 \quad \text{on } \{\Delta_{\max} < \alpha\}.$$

It remains to show $\mathbb{P}(\Delta_{\max} < \alpha_m) \rightarrow 1$.

Step B4 (quantile transform reduces to maximal uniform spacing). Let $F(s) := \int_0^s q(u) du$ be the CDF of S on $[0, L]$. Since $q \geq q_{\min} > 0$, the map F is strictly increasing and invertible onto $[0, 1]$. Define $U_i := F(S_i)$. By the probability integral transform, $U_i \sim \text{Unif}(0, 1)$. Let $U_{(1)} \leq \dots \leq U_{(m)}$ and define spacings $\delta_i := U_{(i+1)} - U_{(i)}$ for $1 \leq i \leq m-1$ and $\delta_{\max} := \max_{1 \leq i \leq m-1} \delta_i$.

Moreover F^{-1} is $(1/q_{\min})$ -Lipschitz: for $0 \leq u < u' \leq 1$, letting $s = F^{-1}(u)$ and $s' = F^{-1}(u')$, the mean value theorem gives $u' - u = F'(\xi)(s' - s) \geq q_{\min}(s' - s)$, hence

$$F^{-1}(u') - F^{-1}(u) \leq \frac{u' - u}{q_{\min}}.$$

Applying this with $u = U_{(i)}$, $u' = U_{(i+1)}$ yields

$$\Delta_i = S_{(i+1)} - S_{(i)} \leq \frac{1}{q_{\min}}(U_{(i+1)} - U_{(i)}) = \frac{1}{q_{\min}}\delta_i,$$

and therefore

$$\Delta_{\max} \leq \frac{1}{q_{\min}}\delta_{\max}. \tag{8}$$

Step B5 (maximal uniform spacing bound). We use a standard discretization/union-bound estimate.

Fact (tail bound for maximal uniform spacing). For every $x \in (0, 1)$,

$$\mathbb{P}(\delta_{\max} > x) \leq \left(\left\lceil \frac{2}{x} \right\rceil\right) \left(1 - \frac{x}{2}\right)^m \leq \left(\frac{2}{x} + 1\right) \exp\left(-\frac{mx}{2}\right).$$

(Proof: if $\delta_{\max} > x$, there is an empty interval of length x ; a grid of step $x/2$ contains an interval of length $x/2$ inside it; union bound over $\lceil 2/x \rceil$ grid intervals; then use $1 - y \leq e^{-y}$.)

Taking $x = \frac{2c \log m}{m}$ with any fixed $c > 1$ gives $\mathbb{P}(\delta_{\max} > x) \rightarrow 0$, hence

$$\delta_{\max} = O_{\mathbb{P}}\left(\frac{\log m}{m}\right).$$

Combining with (8) yields

$$\Delta_{\max} = O_{\mathbb{P}}\left(\frac{\log m}{m}\right).$$

Under the scale assumption $\frac{\log m}{m} = o(\alpha_m)$, we obtain $\Delta_{\max}/\alpha_m \xrightarrow{\mathbb{P}} 0$, equivalently $\mathbb{P}(\Delta_{\max} < \alpha_m) \rightarrow 1$.

Step B6 (finish). By Step B3,

$$\overline{\text{TP}}_0^{[\alpha_m, \beta_m]}(C_m) = 0 \quad \text{on } \{\Delta_{\max} < \alpha_m\},$$

and Step B5 shows $\mathbb{P}(\Delta_{\max} < \alpha_m) \rightarrow 1$. Therefore

$$\overline{\text{TP}}_0^{[\alpha_m, \beta_m]}(C_m) \xrightarrow{\mathbb{P}} 0.$$

This completes the proof of both parts. \square

Proof of Lemma B.5. All distances are Euclidean. We use the point-to-set distance $d_2(z, A)$ and the Hausdorff distance $d_H(A, B)$ as in Background, Section A.4; for notational convenience write $\text{dist}(z, A) := d_2(z, A)$. Recall from Lemma B.5 the definitions of $J_{\eta, j}$, $b_{n, j}$, $\Gamma_{n, \eta}^{(j)}$, $\Gamma_{n, \eta}$, and the clouds $\overline{\mathcal{R}}_{k, \eta}^{(n)}$ and $\mathcal{R}_{k, \eta}^{(n)}$.

Step 1: oracle residual points lie close to the appropriate branch curve. Fix $i \in I_k$ with $Y_{n, i} \in J_{\eta}$ and let $j(i)$ be the unique index such that $X_i \in I_{j(i)}$. Since f is strictly monotone on $I_{j(i)}$ and satisfies $|f'| \geq c_f$ there, its inverse branch $h_{j(i)} : f(I_{j(i)}) \rightarrow I_{j(i)}$ is $(1/c_f)$ -Lipschitz: for $u = f(x)$ and $v = f(x')$ with $x, x' \in I_{j(i)}$, the mean value theorem gives $|u - v| = |f'(\xi)| |x - x'| \geq c_f |x - x'|$, hence

$$|h_{j(i)}(u) - h_{j(i)}(v)| = |x - x'| \leq \frac{1}{c_f} |u - v|.$$

Using $Y_{n, i} = f(X_i) + \sigma_n \varepsilon_i$, we have

$$X_i = h_{j(i)}(f(X_i)) = h_{j(i)}(Y_{n, i} - \sigma_n \varepsilon_i),$$

so by the Lipschitz property,

$$|X_i - h_{j(i)}(Y_{n, i})| \leq \frac{\sigma_n}{c_f} |\varepsilon_i|.$$

Now compare the oracle point $(Y_{n, i}, X_i - m_n(Y_{n, i}))$ to the curve point on the same branch at the same first coordinate,

$$(Y_{n, i}, b_{n, j(i)}(Y_{n, i})) = (Y_{n, i}, h_{j(i)}(Y_{n, i}) - m_n(Y_{n, i})).$$

They share the first coordinate, hence

$$\text{dist}((Y_{n, i}, X_i - m_n(Y_{n, i})), \Gamma_{n, \eta}) \leq |X_i - h_{j(i)}(Y_{n, i})| \leq \frac{\sigma_n}{c_f} |\varepsilon_i|.$$

Taking the maximum over all such i yields

$$\sup_{z \in \overline{\mathcal{R}}_{k, \eta}^{(n)}} \text{dist}(z, \Gamma_{n, \eta}) \leq \frac{\sigma_n}{c_f} \max_{i \in I_k} |\varepsilon_i|. \quad (9)$$

Step 2: each branch curve is well-approximated by its sampled Y -grid. Fix a branch $j \in \{1, \dots, J\}$ and define the index set of test points falling on this branch and inside $J_{\eta, j}$:

$$I_{k, j} := \{i \in I_k : X_i \in I_j, Y_{n, i} \in J_{\eta, j}\}.$$

Define the corresponding sampled grid subset of the branch curve

$$\Gamma_{n, \eta}^{(j), \text{grid}} := \{(Y_{n, i}, b_{n, j}(Y_{n, i})) : i \in I_{k, j}\} \subset \Gamma_{n, \eta}^{(j)}.$$

On the event \mathcal{E}_n from the statement, each nontrivial branch has $I_{k, j} \neq \emptyset$, so the grid set is nonempty.

Let $y \in J_{\eta, j}$. By definition of $\Delta_{n, \eta}^{(j)}$ there exists $i^* \in I_{k, j}$ such that $|y - Y_{n, i^*}| \leq \Delta_{n, \eta}^{(j)}$. Hence,

$$\begin{aligned} \text{dist}((y, b_{n, j}(y)), \Gamma_{n, \eta}^{(j), \text{grid}}) &\leq \|(y, b_{n, j}(y)) - (Y_{n, i^*}, b_{n, j}(Y_{n, i^*}))\|_2 \\ &\leq |y - Y_{n, i^*}| + |b_{n, j}(y) - b_{n, j}(Y_{n, i^*})|. \end{aligned}$$

Since $b_{n, j} = h_j - m_n$, we have for any $y, y' \in J_{\eta, j}$,

$$|b_{n, j}(y) - b_{n, j}(y')| \leq |h_j(y) - h_j(y')| + |m_n(y) - m_n(y')| \leq \frac{1}{c_f} |y - y'| + \omega(|y - y'|),$$

where we used that h_j is $(1/c_f)$ -Lipschitz and $\omega(\cdot)$ is a modulus of continuity for m_n on J_{η} . Therefore,

$$\sup_{(y, b_{n, j}(y)) \in \Gamma_{n, \eta}^{(j)}} \text{dist}((y, b_{n, j}(y)), \Gamma_{n, \eta}^{(j), \text{grid}}) \leq \left(1 + \frac{1}{c_f}\right) \Delta_{n, \eta}^{(j)} + \omega(\Delta_{n, \eta}^{(j)}).$$

Since $\Gamma_{n, \eta}^{(j), \text{grid}} \subset \Gamma_{n, \eta}^{(j)}$, the reverse one-sided term in d_H is 0, and thus

$$d_H(\Gamma_{n, \eta}^{(j), \text{grid}}, \Gamma_{n, \eta}^{(j)}) \leq \left(1 + \frac{1}{c_f}\right) \Delta_{n, \eta}^{(j)} + \omega(\Delta_{n, \eta}^{(j)}). \quad (10)$$

Step 3: estimated residuals are uniformly close to oracle residuals. For each $i \in I_k$ with $Y_{n, i} \in J_{\eta}$,

$$|(X_i - \hat{g}_n^{(-k)}(Y_{n, i})) - (X_i - m_n(Y_{n, i}))| = |\hat{g}_n^{(-k)}(Y_{n, i}) - m_n(Y_{n, i})| \leq \delta_n^{(k)},$$

by Assumption 3.4(ii). Since the first coordinates coincide, this implies the Hausdorff bound

$$d_H(\mathcal{R}_{k, \eta}^{(n)}, \overline{\mathcal{R}}_{k, \eta}^{(n)}) \leq \delta_n^{(k)}. \quad (11)$$

Step 4: assemble the tube bound. Fix $z \in \mathcal{R}_{k, \eta}^{(n)}$. Choose $\bar{z} \in \overline{\mathcal{R}}_{k, \eta}^{(n)}$ with the same index i , so that $\|z - \bar{z}\|_2 \leq \delta_n^{(k)}$ by (11). By (9), there exists a (branch) point $g \in \Gamma_{n, \eta}$ such that $\|\bar{z} - g\|_2 \leq \frac{\sigma_n}{c_f} \max_{i \in I_k} |\varepsilon_i|$. Moreover, if $g \in \Gamma_{n, \eta}^{(j)}$, then (10) provides a grid point $g^{\text{grid}} \in \Gamma_{n, \eta}^{(j), \text{grid}} \subset \Gamma_{n, \eta}^{(j)}$ with

$$\|g - g^{\text{grid}}\|_2 \leq \left(1 + \frac{1}{c_f}\right) \Delta_{n, \eta}^{(j)} + \omega(\Delta_{n, \eta}^{(j)}).$$

Thus by the triangle inequality,

$$\text{dist}(z, \Gamma_{n, \eta}) \leq \|z - \bar{z}\|_2 + \|\bar{z} - g\|_2 + \|g - g^{\text{grid}}\|_2.$$

Taking the supremum over $z \in \mathcal{R}_{k, \eta}^{(n)}$ and then the maximum over branches j yields

$$\sup_{z \in \mathcal{R}_{k, \eta}^{(n)}} \text{dist}(z, \Gamma_{n, \eta}) \leq \max_{1 \leq j \leq J} \left[\frac{\sigma_n}{c_f} \max_{i \in I_{k, j}} |\varepsilon_i| + \delta_n^{(k)} + \left(1 + \frac{1}{c_f}\right) \Delta_{n, \eta}^{(j)} + \omega(\Delta_{n, \eta}^{(j)}) \right].$$

Since (by construction) $\Gamma_{n, \eta}^{(j), \text{grid}} \subset \mathcal{R}_{k, \eta}^{(n)}$ on \mathcal{E}_n up to the same second-coordinate perturbation already accounted for in (11), the reverse one-sided term $\sup_{g \in \Gamma_{n, \eta}} \text{dist}(g, \mathcal{R}_{k, \eta}^{(n)})$ is controlled by the same right-hand side, and hence the same bound holds for the full Hausdorff distance $d_H(\mathcal{R}_{k, \eta}^{(n)}, \Gamma_{n, \eta})$, which is the stated inequality.

Step 5: probability of \mathcal{E}_n and size of $\Delta_{n,\eta}^{(j)}$. Under the branchwise lower-density condition in Assumption 3.3, each set $J_{\eta,j}$ has positive probability mass and the conditional density of Y_n on $J_{\eta,j}$ is bounded below. Hence the event \mathcal{E}_n (that each such branch is hit at least once in fold k) satisfies $\mathbb{P}(\mathcal{E}_n) \rightarrow 1$.

Moreover, for each fixed branch j , conditional on $Y_{n,i} \in J_{\eta,j}$ the points are i.i.d. with density bounded below on the compact interval $J_{\eta,j}$. A standard one-dimensional covering argument then gives

$$\Delta_{n,\eta}^{(j)} = O_{\mathbb{P}}\left(\frac{\log n}{n}\right).$$

Finally, under Assumption 3.4(iii) together with $\frac{\log n}{n} = o(\alpha_n)$ and $\delta_n^{(k)} = o_{\mathbb{P}}(\alpha_n)$, the preceding bound implies $d_H(\mathcal{R}_{X|Y,k,\eta}^{(n)}, \Gamma_{n,\eta}) = o_{\mathbb{P}}(\alpha_n)$, as claimed. \square

B.2. Theorem 3.9

Auxiliary ingredient: binned reverse residuals collapse under fixed noise. The key new feature in the fixed-noise setting is that reverse residuals are averaged within copula bins. After binning, the reverse residual cloud becomes a collection of bin means and collapses (in Hausdorff distance) to the horizontal line $\Gamma = \{(u, 0) : u \in [0, 1]\}$ at a rate that is negligible relative to the mesoscopic window. This collapse forces the windowed H_0 profile in the reverse direction to vanish.

Lemma B.6 (Reverse binned residuals collapse to a line under fixed noise). *Assume the fixed-noise additive-noise model*

$$Y = f(X) + \varepsilon, \quad \varepsilon \perp\!\!\!\perp X, \quad \mathbb{E}[\varepsilon] = 0, \quad \text{Var}(\varepsilon) = \sigma^2 \in (0, \infty),$$

and define the reverse regression target and oracle reverse residual

$$m(y) := \mathbb{E}[X \mid Y = y], \quad \xi := X - m(Y).$$

Fix $K \geq 2$ and a deterministic K -fold partition $\{I_k\}_{k=1}^K$ of $\{1, \dots, n\}$. Let $\hat{g}_n^{(-k)}$ be any cross-fitted estimator of m , and define the cross-fitted reverse residuals

$$r_i^{(X|Y)} := X_i - \hat{g}_n^{(-k(i))}(Y_i), \quad i = 1, \dots, n,$$

where $k(i)$ is the unique fold index such that $i \in I_{k(i)}$.

Copula binning. Assume F_Y is continuous and set $U_i := F_Y(Y_i) \sim \text{Unif}(0, 1)$. Let $B_n \rightarrow \infty$ with $B_n = o(n)$ and form equal-width bins

$$I_{n,b} := \left(\frac{b-1}{B_n}, \frac{b}{B_n}\right], \quad b = 1, \dots, B_n,$$

with bin index sets $J_b := \{i : U_i \in I_{n,b}\}$ and occupancies $N_b := |J_b|$. For each nonempty bin ($N_b \geq 1$), define bin means

$$\bar{u}_b := \frac{1}{N_b} \sum_{i \in J_b} U_i, \quad \bar{r}_b := \frac{1}{N_b} \sum_{i \in J_b} r_i^{(X|Y)}.$$

Let $m_n := \#\{b : N_b \geq 1\}$ and define the binned cloud and target line

$$\hat{\mathcal{R}}_{X|Y}^{(n)} := \{(\bar{u}_b, \bar{r}_b) : 1 \leq b \leq B_n, N_b \geq 1\} \subset (0, 1) \times \mathbb{R}, \quad \Gamma := \{(u, 0) : u \in [0, 1]\}.$$

Mesoscopic window. Let $\tilde{\alpha}_n := \kappa m_n^{-2/3}$ and $\tilde{\beta}_n := c_\beta \tilde{\alpha}_n$ with $\kappa > 0$ and $c_\beta > 1$.

Assumptions. Assume:

1. **Uniform conditional sub-Gaussianity.** There exists $K_0 < \infty$ such that

$$\|\xi \mid Y = y\|_{\psi_2} \leq K_0 \sigma \quad \text{for all } y \text{ in the support of } Y.$$

2. *Bin-averaged regression error is negligible at scale $\tilde{\alpha}_n$. With*

$$\bar{e}_b := \frac{1}{N_b} \sum_{i \in J_b} (\tilde{g}_n^{(-k(i))}(Y_i) - m(Y_i)),$$

we have $\max_{b: N_b \geq 1} |\bar{e}_b| = o_{\mathbb{P}}(\tilde{\alpha}_n)$.

3. *Growth/occupancy.*

$$\frac{B_n^{7/3} \log B_n}{n} \rightarrow 0.$$

Conclusions.

1. *Hausdorff collapse to the line. In Euclidean Hausdorff distance,*

$$d_H(\widehat{\mathcal{R}}_{X|Y}^{(n)}, \Gamma) = o_{\mathbb{P}}(\tilde{\alpha}_n).$$

More quantitatively, one may use the deterministic decomposition

$$d_H(\widehat{\mathcal{R}}_{X|Y}^{(n)}, \Gamma) \leq \underbrace{\max_{b: N_b \geq 1} |\bar{r}_b|}_{\text{vertical tube}} + \underbrace{\sup_{u \in [0, 1]} \min_{b: N_b \geq 1} |u - \bar{u}_b|}_{\text{horizontal grid gap}},$$

and under (A1)–(A3) both terms are $o_{\mathbb{P}}(\tilde{\alpha}_n)$. In particular,

$$\max_{b: N_b \geq 1} |\bar{r}_b| = O_{\mathbb{P}}\left(\sqrt{\frac{B_n \log B_n}{n}}\right) + o_{\mathbb{P}}(\tilde{\alpha}_n), \quad \sup_{u \in [0, 1]} \min_{b: N_b \geq 1} |u - \bar{u}_b| = O_{\mathbb{P}}\left(\frac{1}{B_n}\right).$$

2. *All MST edges fall below the mesoscopic threshold. Let $\varepsilon_1(\cdot), \dots, \varepsilon_{m_n-1}(\cdot)$ be the Euclidean MST edge lengths of a finite cloud. Then*

$$\mathbb{P}\left(\max_{1 \leq j \leq m_n-1} \varepsilon_j(\widehat{\mathcal{R}}_{X|Y}^{(n)}) < \tilde{\alpha}_n\right) \rightarrow 1.$$

3. *Vanishing windowed H_0 profile. Consequently, for any window function $\Psi_{\tilde{\alpha}_n, \tilde{\beta}_n}$ as in Lemma B.3,*

$$\text{TP}_{0, \Psi}^{[\tilde{\alpha}_n, \tilde{\beta}_n]}(\widehat{\mathcal{R}}_{X|Y}^{(n)}) \xrightarrow{\mathbb{P}} 0.$$

Proof of Theorem 3.9.

Proof. We control the two terms defining $\tilde{\Delta}_{0,n}$ separately. For the forward direction, assumption (B2) together with Lemma B.4(i) implies that the forward residual cloud is bulk at the mesoscopic window. Consequently,

$$\text{TP}_0^{[\alpha_n, \beta_n]}(\widehat{\mathcal{R}}_{Y|X}^{(n)}) \xrightarrow{\mathbb{P}} 1.$$

For the reverse direction, consider the binned residual cloud $\widehat{\mathcal{R}}_{X|Y}^{(n)}$. By Lemma B.6, under assumptions (A1)–(A3) its support collapses onto the line Γ . In particular, conclusion (iii) of that lemma yields

$$\text{TP}_0^{[\tilde{\alpha}_n, \tilde{\beta}_n]}(\widehat{\mathcal{R}}_{X|Y}^{(n)}) \xrightarrow{\mathbb{P}} 0.$$

Combining the two convergences,

$$\tilde{\Delta}_{0,n} = \text{TP}_0^{[\alpha_n, \beta_n]}(\widehat{\mathcal{R}}_{Y|X}^{(n)}) - \text{TP}_0^{[\tilde{\alpha}_n, \tilde{\beta}_n]}(\widehat{\mathcal{R}}_{X|Y}^{(n)}) \xrightarrow{\mathbb{P}} 1.$$

Since $\tilde{\Delta}_{0,n} \in [-1, 1]$, bounded convergence implies $\mathbb{E}[\tilde{\Delta}_{0,n}] \rightarrow 1$.

Finally, let $\tau_n \downarrow 0$. Then

$$\mathbb{P}(\widehat{\text{dir}}_n \neq X \rightarrow Y) \leq \mathbb{P}(\tilde{\Delta}_{0,n} \leq \tau_n) \leq \mathbb{P}(|\tilde{\Delta}_{0,n} - 1| \geq 1 - \tau_n) \rightarrow 0,$$

since $1 - \tau_n \rightarrow 1$ and $\tilde{\Delta}_{0,n} \rightarrow 1$ in probability. Hence $\mathbb{P}(\widehat{\text{dir}}_n = X \rightarrow Y) \rightarrow 1$, and moreover

$$\mathbb{P}(\text{abstain}) \leq \mathbb{P}(\tilde{\Delta}_{0,n} \leq \tau_n) \rightarrow 0.$$

□

B.2.1. PROOF OF LEMMAS

Proof of Lemma B.6. Throughout we work with the empirical copula- Y coordinate

$$U_i^{(Y)} := \frac{\text{rank}(Y_i)}{n+1},$$

where $\text{rank}(\cdot)$ and the $(n+1)$ scaling are as in the Background copula pseudo-observations (Section A.3, paragraph ‘‘Ranks and pseudo-observations’’). This choice makes the bin occupancies essentially deterministic; using $U_i = F_Y(Y_i)$ instead only changes the occupancy control (replacing determinism by multinomial concentration), while the remainder of the argument is unchanged.

Write the binned residual mean as

$$\bar{r}_b = \bar{\xi}_b - \bar{e}_b, \quad \bar{\xi}_b := \frac{1}{N_b} \sum_{i \in J_b} \xi_i, \quad \bar{e}_b := \frac{1}{N_b} \sum_{i \in J_b} (\hat{g}_n^{(-k(i))}(Y_i) - m(Y_i)),$$

where $\xi_i := X_i - m(Y_i)$, $J_b := \{i : U_i^{(Y)} \in I_{n,b}\}$ and $N_b := |J_b|$.

Let $B_n \rightarrow \infty$ with $B_n = o(n)$ and define equal-width bins

$$I_{n,b} := \left(\frac{b-1}{B_n}, \frac{b}{B_n} \right], \quad b = 1, \dots, B_n.$$

Since $(U_i^{(Y)})_{i=1}^n$ is a permutation of the deterministic grid $\{1/(n+1), \dots, n/(n+1)\}$, bin membership depends only on ranks and N_b is nonrandom. Writing $U_i^{(Y)} = j/(n+1)$ for a unique $j \in \{1, \dots, n\}$,

$$\frac{b-1}{B_n} < \frac{j}{n+1} \leq \frac{b}{B_n} \iff \frac{(b-1)(n+1)}{B_n} < j \leq \frac{b(n+1)}{B_n}.$$

Hence for $b \leq B_n - 1$,

$$N_b = \left\lfloor \frac{b(n+1)}{B_n} \right\rfloor - \left\lfloor \frac{(b-1)(n+1)}{B_n} \right\rfloor \in \left\{ \left\lfloor \frac{n+1}{B_n} \right\rfloor, \left\lceil \frac{n+1}{B_n} \right\rceil \right\},$$

and for the last bin,

$$N_{B_n} = n - \left\lfloor \frac{(B_n-1)(n+1)}{B_n} \right\rfloor \in \left\{ \left\lfloor \frac{n+1}{B_n} \right\rfloor - 1, \left\lceil \frac{n+1}{B_n} \right\rceil \right\}.$$

Defining

$$N_{\min,n} := \min_{1 \leq b \leq B_n} N_b, \quad m_n := \#\{b : N_b \geq 1\},$$

we obtain

$$N_{\min,n} \geq \left\lfloor \frac{n+1}{B_n} \right\rfloor - 1. \tag{12}$$

Since $B_n = o(n)$ implies $(n+1)/B_n \rightarrow \infty$, there exists n_0 such that for all $n \geq n_0$, $N_{\min,n} \geq 1$, and therefore

$$m_n = B_n, \quad \text{all bins are nonempty.} \tag{13}$$

For each bin define $\bar{u}_b := N_b^{-1} \sum_{i \in J_b} U_i^{(Y)}$. Then $\bar{u}_b \in I_{n,b}$ and

$$\sup_{u \in [0,1]} \min_{b: N_b \geq 1} |u - \bar{u}_b| \leq \frac{1}{B_n}. \quad (14)$$

Fix a bin b . Conditional on $(Y_i)_{i \in J_b}$, the variables $\{\xi_i : i \in J_b\}$ are independent and centered. Assumption (A1) gives the uniform conditional sub-Gaussian bound

$$\|\xi_i | Y_i\|_{\psi_2} \leq K_0 \sigma \quad \text{a.s.}$$

Thus there exists $c > 0$, depending only on K_0 , such that for all $t > 0$,

$$\mathbb{P}(|\bar{\xi}_b| > t \mid (Y_i)_{i \in J_b}) \leq 2 \exp\left(-c N_b \frac{t^2}{\sigma^2}\right). \quad (15)$$

Taking expectations and applying a union bound yields

$$\mathbb{P}\left(\max_{1 \leq b \leq B_n} |\bar{\xi}_b| > t\right) \leq 2B_n \exp\left(-c N_{\min,n} \frac{t^2}{\sigma^2}\right).$$

Choosing $t = \sigma \sqrt{\frac{(1+\delta) \log B_n}{c N_{\min,n}}}$ gives

$$\max_{1 \leq b \leq B_n} |\bar{\xi}_b| = O_{\mathbb{P}}\left(\sigma \sqrt{\frac{\log B_n}{N_{\min,n}}}\right) = O_{\mathbb{P}}\left(\sigma \sqrt{\frac{B_n \log B_n}{n}}\right),$$

using (12).

Let $\Gamma = \{(u, 0) : u \in [0, 1]\}$ and $\widehat{\mathcal{R}}_{X|Y}^{(n)} = \{(\bar{u}_b, \bar{r}_b) : 1 \leq b \leq B_n\}$. Recall d_H and the point-to-set distance $d_2(\cdot, \cdot)$ from the Background (Section A.4). For each (\bar{u}_b, \bar{r}_b) the closest point on Γ is $(\bar{u}_b, 0)$, hence

$$\sup_{z \in \widehat{\mathcal{R}}_{X|Y}^{(n)}} \text{dist}(z, \Gamma) = \max_b |\bar{r}_b|.$$

Conversely, for any $(u, 0) \in \Gamma$,

$$\text{dist}((u, 0), \widehat{\mathcal{R}}_{X|Y}^{(n)}) \leq |u - \bar{u}_b| + |\bar{r}_b| \leq \frac{1}{B_n} + \max_b |\bar{r}_b|,$$

which implies

$$d_H(\widehat{\mathcal{R}}_{X|Y}^{(n)}, \Gamma) \leq \max_b |\bar{r}_b| + \frac{1}{B_n}. \quad (16)$$

Since $\bar{r}_b = \bar{\xi}_b - \bar{e}_b$, combining the above bound with Assumption (A2) gives

$$\max_b |\bar{r}_b| = O_{\mathbb{P}}\left(\sigma \sqrt{\frac{B_n \log B_n}{n}}\right) + o_{\mathbb{P}}(\tilde{\alpha}_n).$$

Using $\tilde{\alpha}_n = \kappa B_n^{-2/3}$ and Assumption (A3), both terms in (16) are $o_{\mathbb{P}}(\tilde{\alpha}_n)$, hence

$$d_H(\widehat{\mathcal{R}}_{X|Y}^{(n)}, \Gamma) = o_{\mathbb{P}}(\tilde{\alpha}_n),$$

which proves conclusion (i).

For $n \geq n_0$, order the points by bin index and consider the path

$$(\bar{u}_1, \bar{r}_1) - \cdots - (\bar{u}_{B_n}, \bar{r}_{B_n}).$$

For each adjacent pair,

$$\|(\bar{u}_{b+1}, \bar{r}_{b+1}) - (\bar{u}_b, \bar{r}_b)\|_2 \leq \frac{2}{B_n} + 2 \max_j |\bar{r}_j| =: \tau_n.$$

Thus there exists a spanning tree whose maximum edge length is at most τ_n , and by the minimum-bottleneck property of MSTs (Background Section A.5, Proposition A.14),

$$\max_j \varepsilon_j(\widehat{\mathcal{R}}_{X|Y}^{(n)}) \leq \tau_n. \quad (17)$$

Since $\tau_n = o_{\mathbb{P}}(\tilde{\alpha}_n)$, this yields conclusion (ii).

On this event all MST edges lie below $\tilde{\alpha}_n$, so $\Psi_{\tilde{\alpha}_n, \tilde{\beta}_n}(\varepsilon_j) = 0$ for all j , and therefore

$$\text{TP}_{0, \Psi}^{[\tilde{\alpha}_n, \tilde{\beta}_n]}(\widehat{\mathcal{R}}_{X|Y}^{(n)}) = 0$$

with probability tending to 1, proving conclusion (iii). \square

B.3. Proof Theorem 3.10

Proof. Write the *ideal* conditional $(1 - \alpha)$ bootstrap critical value as

$$\hat{c}_n(1 - \alpha) := \inf\{t : \widehat{F}_n^*(t) \geq 1 - \alpha\},$$

and define the ideal rejection event $R_n := \{S_n > \hat{c}_n(1 - \alpha)\}$.

Fix $\varepsilon > 0$ and let

$$G_{n, \varepsilon} := \left\{ \sup_t |\widehat{F}_n^*(t) - F_n(t)| \leq \varepsilon \right\}.$$

On $G_{n, \varepsilon}$, by definition of $\hat{c}_n(1 - \alpha)$ we have $\widehat{F}_n^*(\hat{c}_n(1 - \alpha)) \geq 1 - \alpha$, and therefore

$$F_n(\hat{c}_n(1 - \alpha)) \geq \widehat{F}_n^*(\hat{c}_n(1 - \alpha)) - \varepsilon \geq 1 - \alpha - \varepsilon.$$

Consequently,

$$\Pr_{\theta_0}(R_n \mid \mathcal{D}_n) = \Pr_{\theta_0}(S_n > \hat{c}_n(1 - \alpha) \mid \mathcal{D}_n) \leq 1 - F_n(\hat{c}_n(1 - \alpha)) \leq \alpha + \varepsilon \quad \text{on } G_{n, \varepsilon}.$$

Taking expectations and using $\Pr(G_{n, \varepsilon}) \rightarrow 1$ from (A2.1) yields

$$\limsup_{n \rightarrow \infty} \Pr_{\theta_0}(R_n) \leq \alpha + \varepsilon.$$

Since $\varepsilon > 0$ is arbitrary, it follows that $\limsup_{n \rightarrow \infty} \Pr_{\theta_0}(R_n) \leq \alpha$.

Conditional on \mathcal{D}_n , the bootstrap statistics $S_n^{*(b)}$ are i.i.d. with distribution \widehat{F}_n^* . As $B \rightarrow \infty$, the empirical CDF $\widehat{F}_{n, B}^*$ converges uniformly to \widehat{F}_n^* almost surely, implying

$$\hat{c}_{n, B}(1 - \alpha) - \hat{c}_n(1 - \alpha) \xrightarrow{P} 0.$$

Hence the implemented rejection event $\{S_n > \hat{c}_{n, B}(1 - \alpha)\}$ differs from R_n with probability $o(1)$ and therefore inherits the same asymptotic level bound. \square

C. Experimental Details

Methods and baselines. We compare three categories: (i) per-pair unsupervised methods (TRA/TRA-s; RESIT, IGCI, RECI, CDCI; and COMIC, which fits two conditional models per pair and compares codelengths), (ii) supervised baselines (RCC, NCC) trained once per run and then applied to all evaluation pairs, and (iii) external CLI baselines (bQCD with default backend QCQD and $m = 1$ if $n < 200$ else $m = 3$; SLOPPY with AIC/BIC as appropriate).

Supervised training protocol (RCC/NCC). We generate a labeled training set of $N = 500$ synthetic pairs. For each pair, n is drawn from the evaluation grid (or a predefined set covering evaluation sample sizes) to reduce sample-size domain shift. Labels are balanced by swapping (X, Y) for half the pairs. Training pairs use independent seeds and are never reused as evaluation pairs. For NCC, we use a deterministic train/validation split with ratio $r = 0.2$, train up to 500 epochs with early stopping (patience 20), optimize binary cross-entropy, and restore the best validation checkpoint. For RCC, validation is used only for optional offline selection of the number of trees.

C.1. Synthetic experiment protocol

Goals and design principles Synthetic experiments isolate causal-direction identification under progressively harder departures from idealized assumptions. We enforce: (i) controlled generative structure with known ground truth when meaningful; (ii) paired evaluation on identical draws across methods; and (iii) no data leakage by generating supervised training pairs independently of evaluation pairs with explicit splits and fixed seeds.

C.2. Real-world experiments: Tübingen dataset

Goal and scope. We benchmark on curated observational cause–effect pairs where the DGP is unknown and classical identifiability assumptions need not hold. We follow the same global controls as in the synthetic protocol (paired evaluation per dataset, fixed hyperparameters, and strict separation between supervised training and evaluation pairs); this subsection states only what is specific to real data.

Preprocessing. For each selected pair, we extract (X, Y) using the dataset metadata and discard non-finite observations. If a pair contains more than `max_samples` points, we optionally subsample without replacement for compute control; the subsample is drawn once with a fixed RNG seed and reused across all methods on that pair. Beyond these safeguards, we avoid imposing a universal normalization across all methods and instead rely on each method’s recommended preprocessing in the original paper; uniform scaling is considered only in explicit ablations.